

# NLO QCD and electroweak corrections to $Z + \gamma$ production with leptonic Z-boson decays

ANSGAR DENNER<sup>1</sup>, STEFAN DITTMAIER<sup>2</sup>, MARKUS HECHT<sup>2</sup>, CHRISTIAN PASOLD<sup>1</sup>

<sup>1</sup>*Julius-Maximilians-Universität Würzburg, Institut für Theoretische Physik und Astrophysik,  
D-97074 Würzburg, Germany*

<sup>2</sup>*Albert-Ludwigs-Universität Freiburg, Physikalisches Institut,  
D-79104 Freiburg, Germany*

## Abstract:

The next-to-leading-order electroweak corrections to  $pp \rightarrow l^+l^-/\bar{\nu}\nu + \gamma + X$  production, including all off-shell effects of intermediate Z bosons in the complex-mass scheme, are calculated for LHC energies, revealing the typically expected large corrections of tens of percent in the TeV range. Contributions from quark-photon and photon-photon initial states are taken into account as well, but their impact is found to be moderate or small. Moreover, the known next-to-leading-order QCD corrections are reproduced. In order to separate hard photons from jets, both a quark-to-photon fragmentation function á la Glover/Morgan and Frixione's cone isolation are employed. The calculation is available in the form of Monte Carlo programs allowing for the evaluation of arbitrary differential cross sections. Predictions for integrated cross sections are presented for the LHC at 7 TeV, 8 TeV, and 14 TeV, and differential distributions are discussed at 14 TeV for bare muons and dressed leptons. Finally, we consider the impact of anomalous  $ZZ\gamma$  and  $Z\gamma\gamma$  couplings.

# 1 Introduction

The production of a photon with a leptonically decaying  $Z$  boson represents an important process class at hadron colliders such as the Tevatron and the LHC, both as precision test ground of the Standard Model (SM) and as probe for new-physics effects. The investigation of charged lepton pairs at intermediate energy scales with an additional photon is part of the high-precision analysis of inclusive  $Z$ -boson production. Moreover, the production of a photon and a charged lepton pair is the main background to the search for the Higgs-boson decay into a photon and a  $Z$  boson, which can only be measured if the theoretical prediction for the background is well under control [1–4]. At high energies  $Z + \gamma$  production develops a strong sensitivity to potentially existing photon– $Z$ -boson couplings ( $ZZ\gamma$ ,  $Z\gamma\gamma$ ) which are absent in the SM as elementary interactions, so that non-standard  $ZZ\gamma$  and  $Z\gamma\gamma$  couplings can be constrained by investigating  $Z + \gamma$  final states. Such constraints were already reported by the Tevatron experiments [5,6] and further tightened by the LHC experiments ATLAS [7,8] and CMS [9,10]. If the  $Z$  boson decays invisibly into a neutrino pair, the experimental signature is mono-photon production with missing transverse energy, a signal that is particularly interesting in many exotic new-physics models (see, e.g., Refs. [11–14]). Searches for such signals were both carried out at the Tevatron [15,16] and the LHC [17,18]. In none of the experimental analyses of  $Z + \gamma$  production any signs of new physics have been seen so far. In order to carry on those analyses at run 2 of the LHC with higher energy and luminosity, theoretical predictions have to be pushed to a high level of precision, aiming at uncertainties at the level of few percent.

The first calculations for  $Z + \gamma$  production were performed at leading order (LO) in Ref. [19] in 1981. Subsequently next-to-leading-order (NLO) QCD corrections were calculated for on-shell (stable)  $Z$  bosons in Ref. [20] and extended to include leptonic decays in the narrow-width approximation and anomalous couplings in Refs. [21,22]. A Monte Carlo program for  $Z + \gamma$  (and  $W + \gamma$ ) production at NLO QCD was presented in Ref. [23] using amplitudes from Ref. [24], where the leptonic decays of the  $W/Z$  bosons are treated in the narrow-width approximation, while the spin information is retained via decay-angle correlations. In the same approximation the NLO QCD corrections to  $Z + \gamma$  production are also included in the publically available program MCFM [25]. Since the NLO QCD corrections are of the order of 50%, the NNLO QCD corrections were expected to be sizeable. Based on a scale-variation analysis in Ref. [25] they were estimated to be of the order of 5%. Since 2013 the NNLO QCD corrections are available, and predictions for the LHC were published in Ref. [26,27], revealing a residual scale dependence of only  $\sim 2\%$  for the integrated cross section. The NNLO QCD predictions, in particular, include contributions from the loop-induced gluon-fusion process  $gg \rightarrow Z + \gamma$ , which was calculated in the approximation of stable  $Z$  bosons already a long time ago [28].

It is well known that EW corrections can cause sizeable effects at high energies above the EW scale due to the presence of logarithmically enhanced contributions, so-called Sudakov (and subleading) logarithms [29–34]. EW corrections to  $Z + \gamma$  production at hadron colliders have been presented for on-shell  $Z$  bosons in Ref. [35]. Shortly after, in Ref. [36] the EW corrections to  $Z + \gamma$  (and  $W + \gamma$ ) production have been calculated, including the decay of the massive vector bosons in pole approximation.

In this paper we push the existing calculations of EW corrections for  $Z + \gamma$  to the level of complete NLO EW calculations for the full off-shell processes  $pp \rightarrow l^+l^-/\bar{\nu}\nu\gamma + X$ , including all partonic channels ( $q\gamma$  and  $\gamma\gamma$ ) with initial-state (IS) photons. The NLO QCD corrections are rederived as well. In order to attribute collinear photon–jet configurations either to  $Z + \gamma$  or  $Z + \text{jet}$  production, we alternatively employ a quark-to-photon fragmentation function á la Glover and Morgan [37,38] or Frixione’s cone isolation [39].

The paper is organized as follows: Section 2 briefly describes the setup and techniques of our

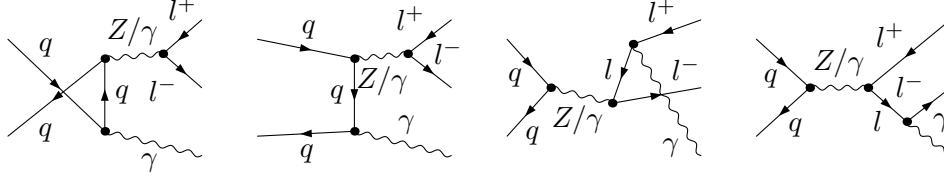


Figure 1: LO Feynman diagrams for the partonic process  $q_i \bar{q}_i \rightarrow l^+ l^- \gamma$ .

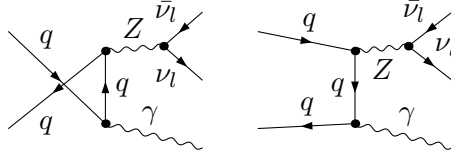


Figure 2: LO Feynman diagrams for the partonic process  $q_i \bar{q}_i \rightarrow \bar{\nu}_l \nu_l \gamma$ .

calculation, referring to the more detailed discussion [40] of  $W + \gamma$  production as much as possible, and contains a survey of the calculated corrections. In Section 3 we discuss our numerical results on total and differential cross sections, both in the SM and including effects of anomalous  $ZZ\gamma$  and  $Z\gamma\gamma$  couplings. Finally, our conclusions are given in Section 4.

## 2 Details of the calculation

The calculation of NLO corrections to  $Z + \gamma$  production follows the methods described in Section 2 of Ref. [40] for  $W + \gamma$  production. In this section we focus on the differences compared to that paper.

### 2.1 General setup

The production of a leptonically decaying  $Z$  boson in association with a hard photon includes two different final states. If the  $Z$  boson decays into two charged leptons the LO partonic process reads

$$q_i \bar{q}_i \rightarrow l^+ l^- \gamma, \quad (2.1)$$

and if the  $Z$  boson decays into two neutrinos it is

$$q_i \bar{q}_i \rightarrow \bar{\nu}_l \nu_l \gamma, \quad (2.2)$$

where  $q_i = u, d, s, c, b$  denotes any light quark. The corresponding LO Feynman diagrams are shown in Figs. 1 and 2. While for the process defined in Eq. (2.1) we assume  $l = e$  or  $\mu$ , the neutrino process includes three families of neutrinos  $\nu_l = \nu_e, \nu_\mu, \nu_\tau$ . For the process where the  $Z$  boson decays into two charged leptons we present results for one single family of final-state (FS) leptons, for the process with neutrinos in the final state we sum the cross sections over all three flavours.

At LO the final state in Eq. (2.1) can also be produced via

$$\gamma \gamma \rightarrow l^+ l^- \gamma, \quad (2.3)$$

which is a pure QED process and does not include any intermediate vector boson. The corresponding LO Feynman diagrams are shown in Fig. 3. Owing to the two photons in the initial state

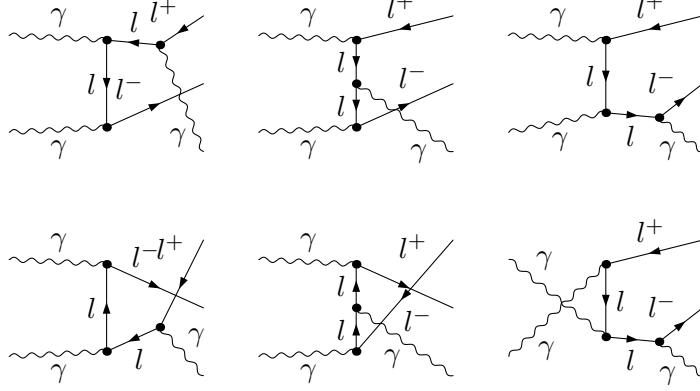


Figure 3: LO Feynman diagrams for the partonic process  $\gamma\gamma \rightarrow l^+l^-\gamma$ .

the partonic cross section is convoluted two times with the very small photon PDFs, so that the contribution to the pp cross section is expected to be small. For this reason we give results for its contribution separately and do not consider NLO EW corrections to this LO process. Since this process only contains charged leptons as intermediate particles there are no QCD corrections at NLO.

We choose to combine QCD and EW corrections to the quark–antiquark-induced channels using the naive product of the relative correction factors, while the quark–photon and the photon–photon contributions are added to the corrected  $q\bar{q}$ -induced cross section,

$$\begin{aligned}\sigma^{\text{NLO}} &= \sigma^{\text{LO}} [(1 + \delta_{\text{QCD}}) (1 + \delta_{\text{EW},q\bar{q}}) + \delta_{\text{EW},q\gamma} + (\delta_{\gamma\gamma})] \\ &= \sigma^{\text{NLO QCD}} (1 + \delta_{\text{EW},q\bar{q}}) + \Delta\sigma_{q\gamma}^{\text{NLO EW}} + (\Delta\sigma_{\gamma\gamma}),\end{aligned}\tag{2.4}$$

where the relative QCD, EW, and photon-induced corrections are defined by

$$\begin{aligned}\delta_{\text{QCD}} &= \frac{\sigma^{\text{NLO QCD}} - \sigma^{\text{LO}}}{\sigma^{\text{LO}}}, & \delta_{\text{EW},q\bar{q}} &= \frac{\Delta\sigma_{q\bar{q}}^{\text{NLO EW}}}{\sigma^0}, \\ \delta_{\text{EW},q\gamma} &= \frac{\Delta\sigma_{q\gamma}^{\text{NLO EW}}}{\sigma^{\text{LO}}}, & \delta_{\gamma\gamma} &= \frac{\Delta\sigma_{\gamma\gamma}}{\sigma^{\text{LO}}},\end{aligned}\tag{2.5}$$

respectively. We have put the photon–photon channel in parentheses to indicate that this channel does not contribute to neutrino production. While the relative QCD and photon-induced corrections are normalized to the LO cross section  $\sigma^{\text{LO}}$ , calculated with LO PDFs, the quark–antiquark-induced EW corrections are normalized to the LO cross section  $\sigma^0$ , calculated with NLO PDFs. By this definition,  $K_{\text{QCD}} = 1 + \delta_{\text{QCD}}$  is the standard QCD  $K$  factor, and the relative quark–antiquark-induced EW corrections  $\delta_{\text{EW},q\bar{q}}$  are practically independent of the PDF set. In case of  $Z + \gamma$  production the purely weak  $\delta_{\text{weak},q\bar{q}}$  and the photonic corrections  $\delta_{\text{phot},q\bar{q}}$  can be separated in a gauge-independent way

$$\delta_{\text{EW},q\bar{q}} = \delta_{\text{weak},q\bar{q}} + \delta_{\text{phot},q\bar{q}}.\tag{2.6}$$

By definition, the photonic corrections comprise all diagrams with photon exchange between fermions in a loop, the corresponding counterterm contributions, and all photon emission effects. All remaining EW corrections to the  $q\bar{q}$  channels furnish the weak corrections. Where appropriate we show the weak corrections and the photonic corrections separately or we show the weak corrections additionally to the EW corrections.

Note that the combination (2.4) also offers an appropriate ansatz for dressing more educated QCD-based predictions with our EW corrections. Specifically, replacing  $\sigma^{\text{NLO QCD}}$  by  $\sigma^{\text{NNLO QCD}}$ , as worked out in Ref. [26], would deliver state-of-the-art predictions based on fixed perturbative orders.

## 2.2 Virtual corrections

We calculate the virtual QCD and EW corrections to the partonic processes defined in Eqs. (2.1) and (2.2). The QCD corrections include contributions from self-energy, vertex, and box (4-point) diagrams only. The virtual EW corrections additionally involve pentagon diagrams. The structural diagrams for the EW NLO corrections for process (2.1) are given in Figs. 4–7, and the pentagons are shown explicitly in Fig. 8. Since the contributions from the LO photon–photon-induced contributions are tiny, we neglect EW corrections to this process.

Since the  $b\bar{b}$  channel contributes only about 3% to the LO cross section, we omit the corresponding EW corrections which we expect to be in the sub per-mille level and therefore negligible.

We have performed two independent loop calculations with two different sets of tools, both making use of traditional methods based on Feynman diagrams. The amplitudes are generated in the 't Hooft–Feynman gauge and algebraically reduced using **MATHEMATICA** programs, producing a standard representation in terms of standard matrix elements containing all spinorial and polarization-dependent objects and Lorentz-invariant coefficients containing the loop integrals. While the standard matrix elements are evaluated in terms of Weyl–van-der-Waerden spinor products following Ref. [41], the loop integrals are computed with the **COLLIER** library [42], which is based on the results of Refs. [43–45]. In one calculation we use **FEYNARTS** 3 [46,47], **FORMCALC** [48], and **POLE** [49] for the generation and reduction of the amplitudes, while the second calculation employs inhouse **MATHEMATICA** routines starting from amplitudes generated with **FEYNARTS** 1 [50].

## 2.3 Real corrections

The real EW corrections to the quark–antiquark channels are induced by the partonic processes

$$q_i \bar{q}_i \rightarrow l^+ l^- \gamma \gamma, \quad (2.7)$$

$$q_i \bar{q}_i \rightarrow \bar{\nu}_l \nu_l \gamma \gamma. \quad (2.8)$$

The Feynman diagrams for (2.7) are shown in Fig. 9. While the production of charged leptons in (2.7) involves photon emission both from the IS and FS, the photons in the neutrino production process (2.8) entirely results from IS radiation (corresponding to the first six diagrams in Fig. 9). In both processes photon bremsstrahlung gives rise to soft and collinear singularities when one of the two photons gets soft or collinear to any charged IS or FS fermion. These singularities are extracted from the phase-space integral and analytically evaluated using the dipole subtraction technique as formulated for photons in Refs. [51,52]. While the soft singularities completely cancel against the virtual corrections, the remaining collinear IS singularities can be absorbed into the proton PDFs. In view of collinear singularities from photon radiation off FS leptons we have considered two scenarios, called the collinear-safe (CS) and non-collinear-safe (NCS) case in Ref. [40]. In detail our calculation closely follows Section 2.3.1 of Ref. [40], where the corresponding part of our NLO calculation for  $W + \gamma$  production is described.

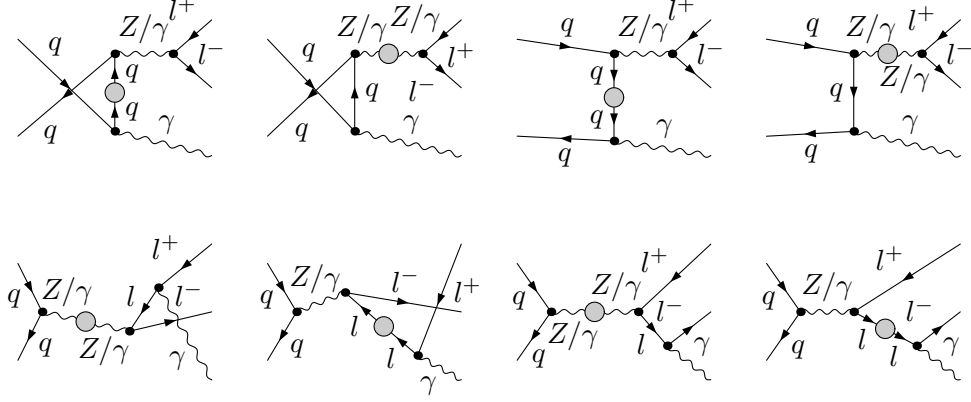


Figure 4: Self-energy corrections to the partonic process  $q_i \bar{q}_i \rightarrow l^+ l^- \gamma$ .

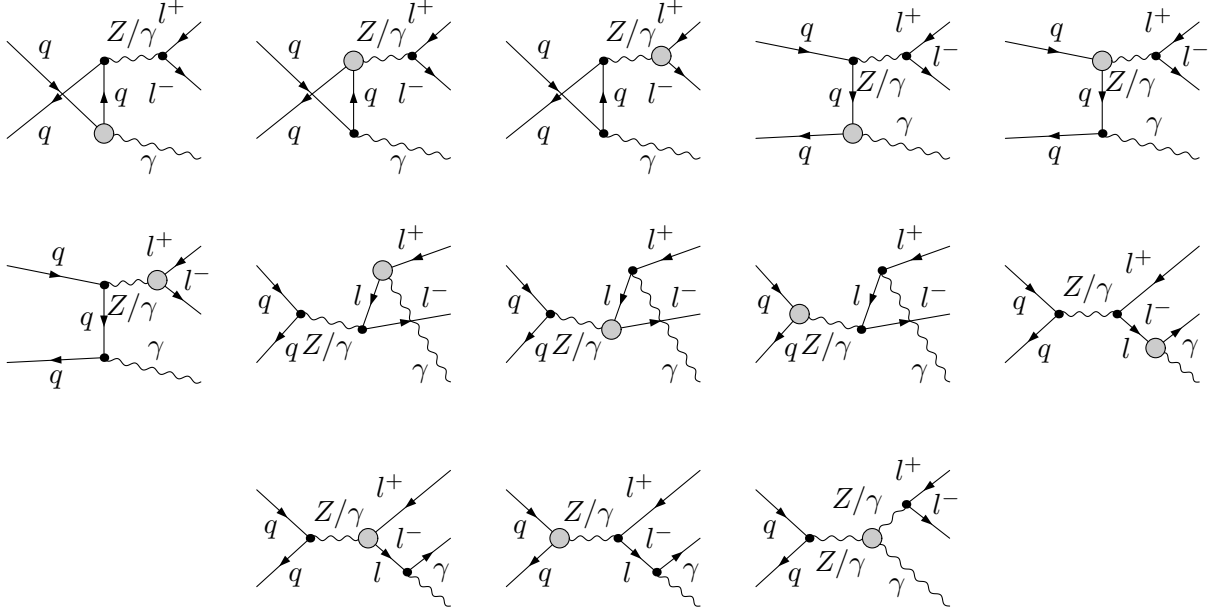


Figure 5: Vertex corrections to the partonic process  $q_i \bar{q}_i \rightarrow l^+ l^- \gamma$ .

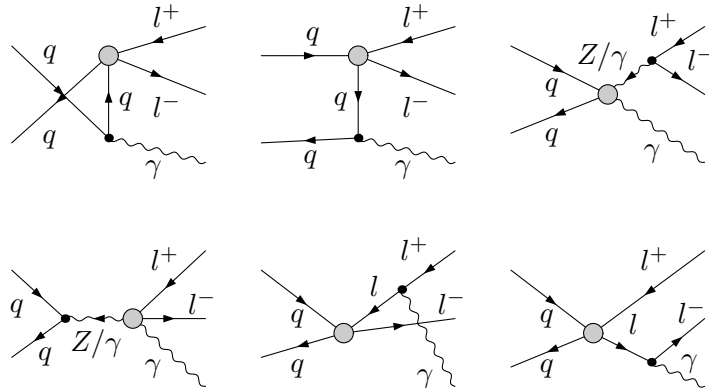


Figure 6: Box corrections to the partonic process  $q_i \bar{q}_i \rightarrow l^+ l^- \gamma$ .

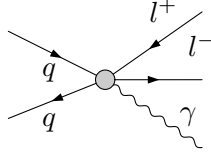


Figure 7: Pentagon corrections for the partonic process  $q_i \bar{q}_i \rightarrow l^+ l^- \gamma$ .

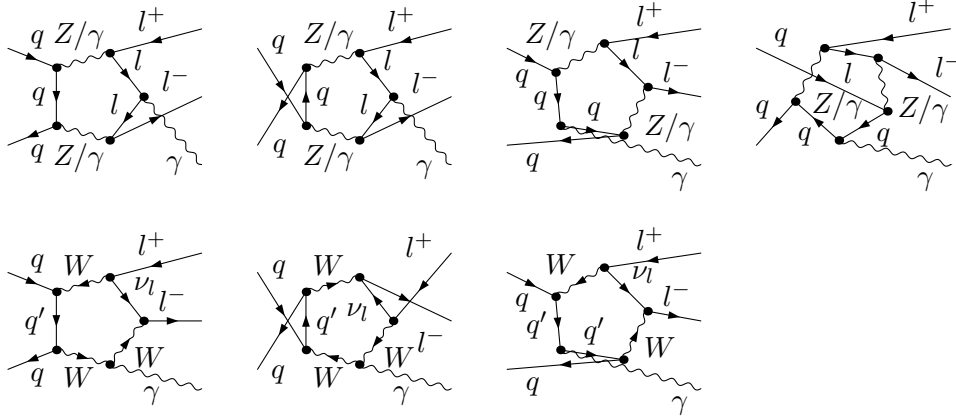


Figure 8: Explicit pentagon diagrams for the partonic process  $q_i \bar{q}_i \rightarrow l^+ l^- \gamma$ .

For the real QCD corrections we have to consider the partonic channels

$$\begin{aligned}
 q_i \bar{q}_i &\rightarrow l^+ l^- \gamma g, \\
 q_i g &\rightarrow l^+ l^- \gamma q_i, \\
 \bar{q}_i g &\rightarrow l^+ l^- \gamma \bar{q}_i,
 \end{aligned}
 \tag{2.9}$$

for the process involving charged leptons and the channels

$$\begin{aligned}
 q_i \bar{q}_i &\rightarrow \bar{\nu}_l \nu_l \gamma g, \\
 q_i g &\rightarrow \bar{\nu}_l \nu_l \gamma q_i, \\
 \bar{q}_i g &\rightarrow \bar{\nu}_l \nu_l \gamma \bar{q}_i
 \end{aligned}
 \tag{2.10}$$

for the process with neutrinos in the final state. The corresponding Feynman diagrams to the first process in (2.9) are shown in Fig. 10. The diagrams for the gluon-induced contributions can be derived via crossing symmetries. The calculation of these corrections is completely analogous to the one described in Sections 2.3.2 and 2.3.3 of Ref. [40], i.e. we again use dipole subtraction [53, 54] to treat soft and collinear singularities resulting from collinear IS splittings. Since the final states in (2.9) and (2.10) contain a photon and a jet, which can become collinear, we apply two different methods for the treatment of collinear photon-jet configurations. We use the concept of democratic clustering in combination with a quark-to-photon fragmentation function as introduced in Refs. [37, 38] and the Frixione isolation scheme [39] as an alternative. Both schemes identify a collinear photon-jet system as a photon if the photonic energy content in this system exceeds a certain fraction of its total energy, in order to define the  $Z + \gamma$  contribution in the process  $pp \rightarrow Z + \gamma + \text{jet} + X$ . In the same spirit, the  $Z + \text{jet}$  contribution was defined in Refs. [55, 56], where NLO QCD+EW corrections to the complementary processes  $pp \rightarrow Z(\rightarrow l^+ l^- / \bar{\nu} \nu) + \text{jet} + X$  were calculated.

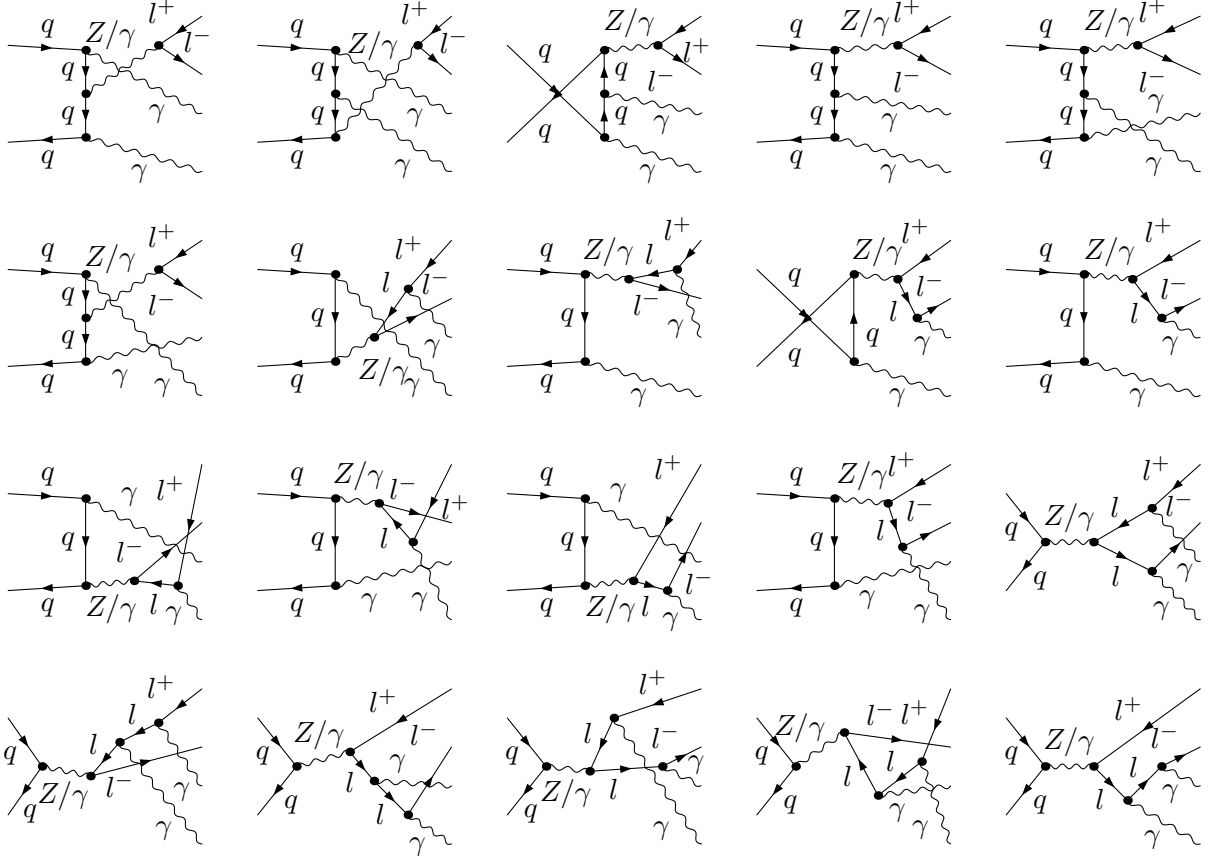


Figure 9: Feynman diagrams of the quark–antiquark-induced real EW corrections for the partonic process  $q_i \bar{q}_i \rightarrow l^+ l^- \gamma$ .

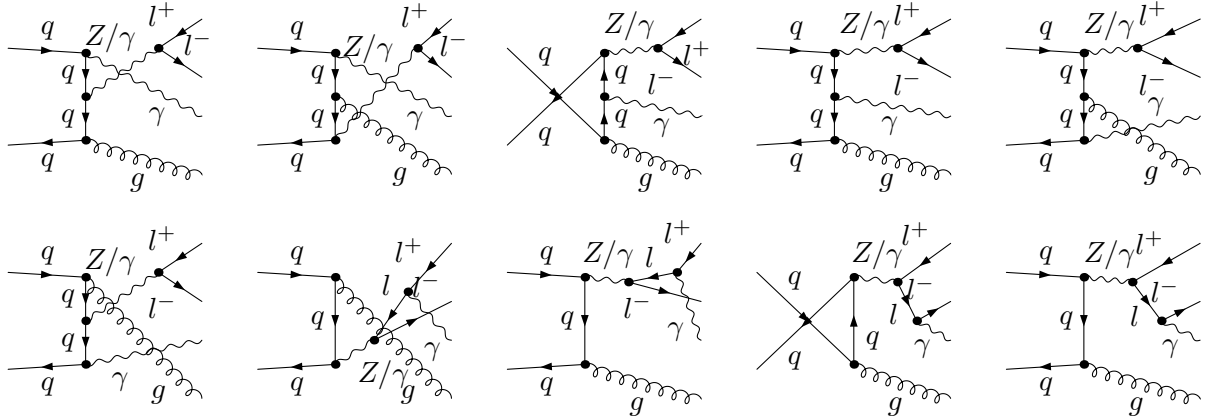


Figure 10: Feynman diagrams of the quark–antiquark-induced real QCD corrections for the partonic process  $q_i \bar{q}_i \rightarrow l^+ l^- \gamma$ .



The photon-induced EW corrections include the partonic channels

$$\begin{aligned} q_i \gamma &\rightarrow l^+ l^- \gamma q_i, \\ \bar{q}_i \gamma &\rightarrow l^+ l^- \gamma \bar{q}_i, \end{aligned} \quad (2.11)$$

and

$$\begin{aligned} q_i \gamma &\rightarrow \bar{\nu}_l \nu_l \gamma q_i, \\ \bar{q}_i \gamma &\rightarrow \bar{\nu}_l \nu_l \gamma \bar{q}_i. \end{aligned} \quad (2.12)$$

The Feynman diagrams for (2.11) can be derived from the diagrams in Fig. 9 via crossing of a FS photon to the IS and a quark or antiquark into the FS. Besides soft and collinear singularities from photon radiation off fermions and collinear photon–jet configurations the photon-induced EW corrections additionally include singularities from the collinear splittings  $\gamma \rightarrow f \bar{f}^*$  and  $f \rightarrow f \gamma^*$ . Our treatment of these singularities follows Sections 3 and 5 of Ref. [52]. Some details can also be found in Section 2.3.3 of Ref. [40].

### 3 Numerical results

#### 3.1 Input parameters and setup

The relevant SM input parameters are

$$\begin{aligned} G_\mu &= 1.1663787 \times 10^{-5} \text{ GeV}^{-2}, & \alpha(0) &= 1/137.035999074, & \alpha_s(M_Z) &= 0.119, \\ M_H &= 125 \text{ GeV}, & m_\mu &= 105.6583715 \text{ MeV}, & m_t &= 173.07 \text{ GeV}, \\ M_W^{\text{OS}} &= 80.385 \text{ GeV}, & \Gamma_W^{\text{OS}} &= 2.085 \text{ GeV}, \\ M_Z^{\text{OS}} &= 91.1876 \text{ GeV}, & \Gamma_Z^{\text{OS}} &= 2.4952 \text{ GeV}. \end{aligned} \quad (3.1)$$

All parameters but  $\alpha_s(M_Z)$ , which is provided by the PDF set, are extracted from Ref. [57]. The masses of all quarks but the top quark are set to zero.

Owing to the presence of an on-shell external photon, we always take one electromagnetic coupling constant  $\alpha$  at zero momentum transfer,  $\alpha = \alpha(0)$ . For all other couplings, e.g. the Z-boson–fermion or additional photon–fermion couplings, we determine the electromagnetic coupling constant in the  $G_\mu$  scheme, where  $\alpha$  is defined in terms of the Fermi constant,

$$\alpha_{G_\mu} = \frac{\sqrt{2}}{\pi} G_\mu M_W^2 \left( 1 - \frac{M_W^2}{M_Z^2} \right). \quad (3.2)$$

This definition effectively absorbs some universal corrections into the LO contributions, such as those associated with the evolution of  $\alpha$  from zero momentum transfer to the electroweak scale and corrections related to the  $\rho$ -parameter. In this scheme large fermion-mass logarithms are effectively resummed leading to an independence of logarithms of the light fermion masses [58] (see also the discussion in the “EW dictionary” in Ref. [59]). Using this mixed scheme the squared LO amplitude is proportional to  $\alpha(0)\alpha_{G_\mu}^2$ . In the relative EW corrections we set the additional coupling factor  $\alpha$  to  $\alpha_{G_\mu}$ , because this coupling is adequate for the most pronounced EW corrections which are caused by soft/collinear weak gauge-boson exchange at high energies (EW Sudakov logarithms, etc.).

We use the complex-mass scheme [60–62] to treat the Z-boson resonance by introducing complex vector-boson masses  $\mu_{W,Z}$  according to

$$M_W^2 \rightarrow \mu_W^2 = M_W^2 - i M_W \Gamma_W, \quad M_Z^2 \rightarrow \mu_Z^2 = M_Z^2 - i M_Z \Gamma_Z \quad (3.3)$$

with constant decay widths  $\Gamma_{W,Z}$ . However, at LEP and the Tevatron the on-shell (OS) masses of the vector bosons were measured, which correspond to running widths. Therefore, the OS masses  $M_W^{\text{OS}}$ ,  $M_Z^{\text{OS}}$  and widths  $\Gamma_W^{\text{OS}}$ ,  $\Gamma_Z^{\text{OS}}$  have to be converted to the pole values using the relations [63]

$$M_V = M_V^{\text{OS}} / \sqrt{1 + (\Gamma_V^{\text{OS}} / M_V^{\text{OS}})^2}, \quad \Gamma_V = \Gamma_V^{\text{OS}} / \sqrt{1 + (\Gamma_V^{\text{OS}} / M_V^{\text{OS}})^2} \quad (V = W, Z), \quad (3.4)$$

resulting in

$$\begin{aligned} M_W &= 80.3580 \dots \text{ GeV}, & \Gamma_W &= 2.0843 \dots \text{ GeV}, \\ M_Z &= 91.1535 \dots \text{ GeV}, & \Gamma_Z &= 2.4943 \dots \text{ GeV}. \end{aligned} \quad (3.5)$$

Calculating the hadronic cross section, we employ the NNPDF2.3QED PDF set [64], which includes a photon PDF, QED contributions to parton evolution and the two-loop running of  $\alpha_s$  for five active flavours ( $n_f = 5$ ). Following the arguments of Ref. [65], we apply a DIS-like factorization scheme for the QED corrections (see, e.g., Ref. [66]), but an  $\overline{\text{MS}}$  prescription for the QCD corrections as demanded by the NNPDF2.3QED PDF set.

Strictly speaking, the choice of the factorization scheme of the QED corrections is ambiguous for the NNPDF2.3QED PDF set. Therefore, we have performed the calculation for the QED corrections also using the  $\overline{\text{MS}}$  factorization scheme. The results for the integrated cross sections differ from those obtained with the DIS-like scheme by less than 0.05% both for the relative EW corrections and the photon-induced corrections relative to the leading order. Also in all considered distributions the changes are well below 0.1% and thus phenomenologically negligible.

The factorization and the renormalization scales  $\mu_F, \mu_R$  are set equal throughout our calculation. Following Refs. [67, 68], we choose the scales as

$$\mu_F^2 = \mu_R^2 = \frac{1}{2} \left( M_Z^2 + p_{T,Z}^2 + p_{T,\gamma_1}^2 + p_{T,\gamma_2/\text{jet}}^2 \right), \quad (3.6)$$

where  $p_{T,Z}$  is the transverse momentum of the massive vector boson defined by

$$p_{T,Z} = \begin{cases} |\mathbf{p}_{T,\bar{\nu}_l} + \mathbf{p}_{T,\nu_l}| & \text{for } pp \rightarrow \bar{\nu}_l \nu_l \gamma, \\ |\mathbf{p}_{T,l^+} + \mathbf{p}_{T,l^-}| & \text{for } pp \rightarrow l^+ l^- \gamma, \end{cases} \quad (3.7)$$

and  $p_{T,a} = |\mathbf{p}_{T,a}|$  denotes the absolute value of the transverse three-momentum  $\mathbf{p}_{T,a}$  of particle  $a$ . The photons  $\gamma_1$  and  $\gamma_2$  are ordered so that  $p_{T,\gamma_1} > p_{T,\gamma_2}$  and we call the hardest photon the one with the highest transverse momentum. In LO the transverse momenta  $p_{T,\gamma_2/\text{jet}}$  vanish.

The QCD scale uncertainty of  $Z + \gamma$  production has already been investigated in various publications such as in Refs. [21, 23, 25]. Varying the scale by a factor of two the scale dependence was found to be of the order of 5% at NLO QCD in Ref. [25]. Meanwhile NNLO QCD corrections have been calculated [26] and found to contribute another 6% on top of the NLO QCD prediction for the integrated cross section. The corresponding scale uncertainty is reduced to 2% at NNLO QCD. Note, however, that the scale definition slightly differs from ours.

### 3.2 Phase-space cuts and event selection

The processes  $pp \rightarrow \bar{\nu}_l \nu_l + \gamma + X$  and  $pp \rightarrow l^+ l^- + \gamma + X$  require the recombination of FS photons with FS partons and, in case of the second process, of FS photons with charged leptons in regimes of phase space where photon and parton/lepton are collinear. Furthermore, we impose several cuts to account for the detector acceptance. The phase-space cuts and the event selection are inspired by the recent ATLAS and CMS papers [7–10] analyzing  $W\gamma$  and  $Z\gamma$  final states.

### 3.2.1 Recombination

Recombination of a photon and a FS particle is based on the Euclidean distance in the  $y$ - $\phi$  plane,  $R_{ij} = \sqrt{(y_i - y_j)^2 + \phi_{ij}^2}$ , where  $y = \frac{1}{2} \ln [(E + p_L) / (E - p_L)]$  denotes the rapidity. Here,  $E$  is the energy and  $p_L$  the longitudinal momentum of the respective particle along the beam axis. Furthermore,  $\phi_{ij}$  refers to the angle between the particles  $i$  and  $j$  in the plane perpendicular to the beams. The recombination is performed as follows:

1. If we consider “bare” muons, a photon and a charged (anti)lepton are never recombined. Otherwise recombination is applied if  $R_{l\pm\gamma} < 0.1$ , and the four-momenta of photon and lepton are added. If the separation in  $R$  between the photon and each of the two leptons is smaller than 0.1 at the same time, the photon is recombined with the lepton that has a smaller  $R_{l\gamma}$  separation. In case of two photons in the final state, first the photon with the smaller  $R_{l\pm\gamma}$  is recombined.
2. Two photons are recombined if  $R_{\gamma\gamma} < 0.1$ .
3. Using the method of democratic clustering, a photon and a jet are recombined if their distance becomes  $R_{\gamma\text{jet}} < R_0 = 0.5$ . After recombination, the energy fraction  $z_\gamma = E_\gamma / (E_\gamma + E_{\text{jet}})$  of the photon inside the photon-jet system is determined. If  $z_\gamma$  is smaller than  $z_{\text{cut}} = 0.9$  the event is regarded as a part of the process  $Z + \text{jet}$  and therefore rejected.

The case where more than two particles are recombined is excluded by our basic cuts. Results are presented for “bare” muons and for photon recombination with leptons. The latter results hold for electrons as well as for muons, since the lepton-mass logarithms cancel as dictated by the KLN theorem [69, 70].

If alternatively the Frixione isolation scheme is applied, step 3 is replaced as follows:

- 3'. If  $R_{\gamma\text{jet}} < R_0 = 0.5$  the photon and the jet are recombined and the event is only accepted if it respects the inequality

$$p_{T,\text{jet}} < \varepsilon p_{T,\gamma} \left( \frac{1 - \cos(R_{\gamma\text{jet}})}{1 - \cos(R_0)} \right). \quad (3.8)$$

This condition replaces the condition  $z_\gamma > z_{\text{cut}}$  used in the approach based on democratic clustering and the quark-to-photon fragmentation function. Neglecting the difference between  $E$  and  $p_T$  and taking into account that  $R_{\gamma\text{jet}} \sim R_0$  for the critical events, the two parameters  $z_{\text{cut}}$  and  $\varepsilon$  can be related by

$$z_{\text{cut}} \approx \frac{1}{1 + \varepsilon}. \quad (3.9)$$

With this equation we get  $\varepsilon = 0.11$  for  $z_{\text{cut}} = 0.9$ .

### 3.2.2 Basic cuts

After recombination, we define events for  $pp \rightarrow l^+ l^- + \gamma + X$  by the following cut procedure:

1. We demand two charged leptons with transverse momentum  $p_{T,l^\pm} > 25$  GeV.
2. We require at least one photon with transverse momentum  $p_{T,\gamma} > 15$  GeV that is isolated from the charged leptons with a distance  $R_{l\pm\gamma} > 0.7$ .

3. The charged leptons and the hardest photon passing the cuts at step 2 have to be central, i.e. their rapidities have to be in the range  $|y| < 2.5$ .
4. Only events with an invariant mass of the lepton pair  $M_{l+l-} > 40 \text{ GeV}$  are accepted, where

$$M_{l+l-} = \sqrt{(p_{l+} + p_{l-})^2}, \quad (3.10)$$

and  $p_{l+}$  and  $p_{l-}$  are the four-vectors of the charged leptons.

Events for the process  $pp \rightarrow \bar{\nu}_l \nu_l + \gamma + X$  are defined by the following cut procedure:

1. We demand a missing transverse momentum  $\cancel{p}_T > 90 \text{ GeV}$ , where  $\cancel{p}_T$  is given by

$$\cancel{p}_T = |\mathbf{p}_{T,\bar{\nu}_l} + \mathbf{p}_{T,\nu_l}|. \quad (3.11)$$

2. We require at least one photon with transverse momentum  $p_{T,\gamma} > 100 \text{ GeV}$ .
3. The hardest photon passing the cuts at step 2 has to be central, i.e. its rapidity has to be in the range  $|y_\gamma| < 2.5$ .
4. Only events with  $\phi_{\gamma,\text{miss}} > 2.6$  are taken into account, where  $\phi_{\gamma,\text{miss}}$  is the angle between the missing transverse momentum  $\cancel{\mathbf{p}}_T = \mathbf{p}_{T,\bar{\nu}_l} + \mathbf{p}_{T,\nu_l}$  and the hardest photon momentum in the plane perpendicular to the beam axis.

We present results with and without applying a jet veto. Applying a jet veto means that all events including a FS jet with  $p_{T,\text{jet}} > 100 \text{ GeV}$  are discarded. Experimentally a jet is required to lie in the rapidity range  $|y_{\text{jet}}| < 4.4$ . In our calculation we do not restrict the rapidity range of the vetoed jets, since the related impact on the cross section is very small and lies within the theoretical uncertainty.

### 3.3 Dilepton + photon production: $pp \rightarrow l^+ l^- + \gamma + X$

#### 3.3.1 Results on total cross sections

In Table 1 we present the LO cross sections  $\sigma^{\text{LO}}$  for different pp centre-of-mass energies  $\sqrt{s}$  and different types of relative corrections  $\delta$  defined in (2.5) for  $pp \rightarrow l^+ l^- + \gamma + X$ . As already mentioned in Sect. 2.1, we split the EW corrections according to Eq. (2.6) into the photonic and the weak contributions  $\delta_{\text{phot}}$  and  $\delta_{\text{weak}}$ , respectively. For the photonic corrections resulting from the quark–antiquark-induced channels we show results for the CS and NCS scenarios. Results for the EW corrections originating from photon-induced channels and for the QCD corrections are listed with and without a jet veto. Furthermore, we present results obtained by applying democratic clustering in combination with a quark-to-photon fragmentation function and the Frixione isolation scheme indicated by “frag” and “Frix”, respectively. The different relative corrections are not particularly sensitive to the collider energy. The largest variation ( $\sim 60\text{--}68\%$ ) occurs in the QCD corrections. A jet veto allowing a maximal jet transverse momentum of  $100 \text{ GeV}$  does not diminish the QCD corrections considerably, since energy scales dominating the integrated cross section are much lower for our setup, which allows for photons (leptons) down to transverse-momentum values of  $15 (25) \text{ GeV}$ . The gluon-induced channels (not separately shown) contribute only about a tenth to the QCD corrections at an energy of  $14 \text{ TeV}$  and even less at lower collider energies. The results obtained with the fragmentation function and the Frixione isolation scheme differ by  $0.5\text{--}1\%$  for the QCD corrections. The photonic corrections to the quark–antiquark channels are about  $-2.7\%$

$pp \rightarrow l^+l^-\gamma + X$			
$\sqrt{s}/\text{TeV}$	7	8	14
$\sigma^{\text{LO}}/\text{fb}$	728.85(4)	818.43(5)	1317.4(1)
$\delta_{\text{phot},q\bar{q}}^{\text{NCS}}/\%$	-4.79(2)	-4.76(2)	-4.70(2)
$\delta_{\text{phot},q\bar{q}}^{\text{CS}}/\%$	-2.74(1)	-2.73(1)	-2.70(1)
$\delta_{\text{weak},q\bar{q}}/\%$	-0.73	-0.73	-0.74
$\delta_{\text{EW},q\gamma}^{\text{frag}}/\%$	0.04	0.04	0.04
$\delta_{\text{EW},q\gamma}^{\text{veto, frag}}/\%$	0.02	0.02	0.02
$\delta_{\text{EW},q\gamma}^{\text{Frix}}/\%$	0.04	0.04	0.05
$\delta_{\text{EW},q\gamma}^{\text{veto, Frix}}/\%$	0.02	0.02	0.02
$\delta_{\gamma\gamma}/\%$	0.27	0.26	0.22
$\delta_{\text{QCD}}^{\text{frag}}/\%$	61.48(5)	62.90(5)	67.58(5)
$\delta_{\text{QCD}}^{\text{Frix}}/\%$	60.62(4)	61.96(5)	67.09(7)
$\delta_{\text{QCD}}^{\text{veto, frag}}/\%$	58.76(5)	59.69(5)	63.11(6)
$\delta_{\text{QCD}}^{\text{veto, Frix}}/\%$	57.76(4)	58.86(6)	62.33(5)

Table 1: Integrated cross sections and relative corrections for  $pp \rightarrow l^+l^-\gamma + X$  at different LHC energies. The EW corrections to the quark–antiquark annihilation channels are split into purely weak and photonic corrections. The photonic corrections are provided with (CS) and without (NCS) lepton–photon recombination. Contributions from the photon-induced channels and QCD corrections are shown with a jet veto (veto) as well as without a jet veto, using a fragmentation function (frag) or the Frixione isolation criterion (Frix) to separate photons and jets. The numbers in parentheses denote the integration errors in the last digits. This error is omitted if it is negligible at the given accuracy.

and  $-4.7\%$  for the CS and the NCS case, respectively. The weak corrections are about  $-0.7\%$  almost independent of the collider energy. The quark–photon-induced corrections contribute less than  $0.05\%$  with and without a jet veto and, thus, are phenomenologically negligible. The photon–photon-induced channel contributes with  $\sim 0.25\%$ .

In summary, the quark–antiquark-induced EW corrections to the integrated cross sections are small compared to the NLO QCD corrections. Nevertheless, in particular, the photonic corrections become relevant in future analyses, since they are of the order of several percent, i.e. larger than the residual scale uncertainty of the NNLO QCD corrections. The photon-induced EW corrections are at the per-mille level and not significant for experimental cross-section measurements. However, larger effects appear in differential distributions, as demonstrated in the following.

### 3.3.2 Results on transverse-momentum distributions

In the following we present differential distributions including QCD and EW corrections to  $pp \rightarrow l^+l^- + \gamma + X$  for a pp centre-of-mass energy of 14 TeV. For each distribution the relative EW corrections of the  $q\bar{q}$ ,  $q\gamma$ , and  $\gamma\gamma$  channels as well as the QCD corrections with and without a jet veto are shown. Since the difference between Frixione isolation and the quark-to-photon fragmentation function is of the order of 1% for the integrated cross section and distributions, and therefore not

very significant, we only show results obtained with the quark-to-photon fragmentation function. For  $Z + \gamma$  production the purely weak and the photonic corrections can be separated in a gauge-independent way. In order to show the impact of the weak corrections  $\delta_{\text{weak}, q\bar{q}}$  we plot them additionally to the full EW corrections.

In Fig. 11 we show results on the transverse-momentum distributions of the hardest photon (within cuts) and of the Z boson (defined in Eq. (3.7)). Both distributions receive large QCD corrections in the region of high transverse momenta. This is due to the fact that at NLO QCD new channels appear ( $qg \rightarrow l^+ l^- \gamma q$ ) causing large corrections, especially in the high- $p_T$  tails. However, these large corrections originate from events with hard jets. These events should preferably be considered as part of  $Z + \text{jet}$  rather than  $Z + \gamma$  production. Therefore we additionally show distributions for the case of a jet veto discarding events with  $p_{T, \text{jet}} > 100 \text{ GeV}$ . The jet veto suppresses the large QCD corrections at high transverse momenta. The  $p_T$  distributions of the photon and the Z boson receive large negative EW corrections, which predominantly originate from so-called EW Sudakov logarithms included in the weak corrections  $\delta_{\text{weak}, q\bar{q}}$ . In case of the  $p_{T, \gamma}$  distribution the CS and the NCS cases hardly differ, since the recombination of the second photon and a collinear lepton hardly influences the transverse momentum of the hardest photon. By contrast, the CS and the NCS cases differ in the  $p_{T, Z}$  distribution. This is due to the fact that the transverse momentum of the Z boson is reconstructed from the momenta of the charged leptons which are sensitive to the recombination with a collinearly radiated photon. The quark-photon-induced corrections are below 10% in both distributions and almost vanish in case of a jet veto. The photon-photon-induced corrections grow up to 4% at  $p_{T, Z} = 1 \text{ TeV}$ . They are not affected by the jet veto, since there is no jet in the FS. In summary, the EW corrections are much smaller than the QCD corrections if no jet veto is applied, but sizeable. In case of a jet veto they even become the leading corrections in the high-transverse-momentum tails.

The transverse-momentum distributions of the two charged leptons are shown in Fig. 12. The QCD corrections turn out to be of the order of 150% at 100 GeV and decrease to 50% at 1 TeV if no jet veto is applied. In case of a jet veto the corrections are still large (100%) in the low  $p_T$ -range and drop to -50% at 1 TeV. The transverse-momentum distribution of each charged lepton receives large negative weak corrections originating from the Sudakov logarithms, reaching -15% at 1 TeV. The difference between the CS and the NCS EW corrections is roughly 6%. The collinear radiation of photons off FS charged leptons shifts the lepton transverse momentum to smaller values, causing negative corrections. Recombining the charged lepton with the collinear photon partly compensates this effect, which is why the CS corrections are smaller. The quark-photon-induced corrections are below 5% and almost vanish in case of a jet veto. The photon-photon-induced correction grows up to more than 10% at 1 TeV. In the high- $p_T$  tail the EW corrections are of the same order of magnitude as the QCD corrections with and without a jet veto. The transverse-momentum distributions of the two charged leptons and the corresponding corrections do not differ significantly.

The large EW and photon-induced corrections at high transverse momenta and invariant masses raise the question of the corresponding uncertainties. The leading EW corrections in this region arise from the Sudakov double logarithms which are of purely weak origin and known to exponentiate [33]. Therefore, we can estimate the uncertainty from the missing NNLO EW corrections as the square of the relative NLO weak corrections  $(\delta_{\text{weak}, q\bar{q}})^2$ , which amounts to 16% for the  $p_{T, \gamma}$   $p_{T, Z}$  distributions and 2% for the distributions in the transverse momenta of the leptons at 1 TeV. This estimate is in agreement with calculations of NNLO EW Sudakov corrections for processes with on-shell vector bosons [71].

At large Bjorken- $x$  the photon-PDF carries large uncertainties of the order of 100% [64]. This can be translated to an uncertainty for the photon-induced processes where these yield large contributions. Therefore, the contributions of the photon-induced processes should be viewed as an

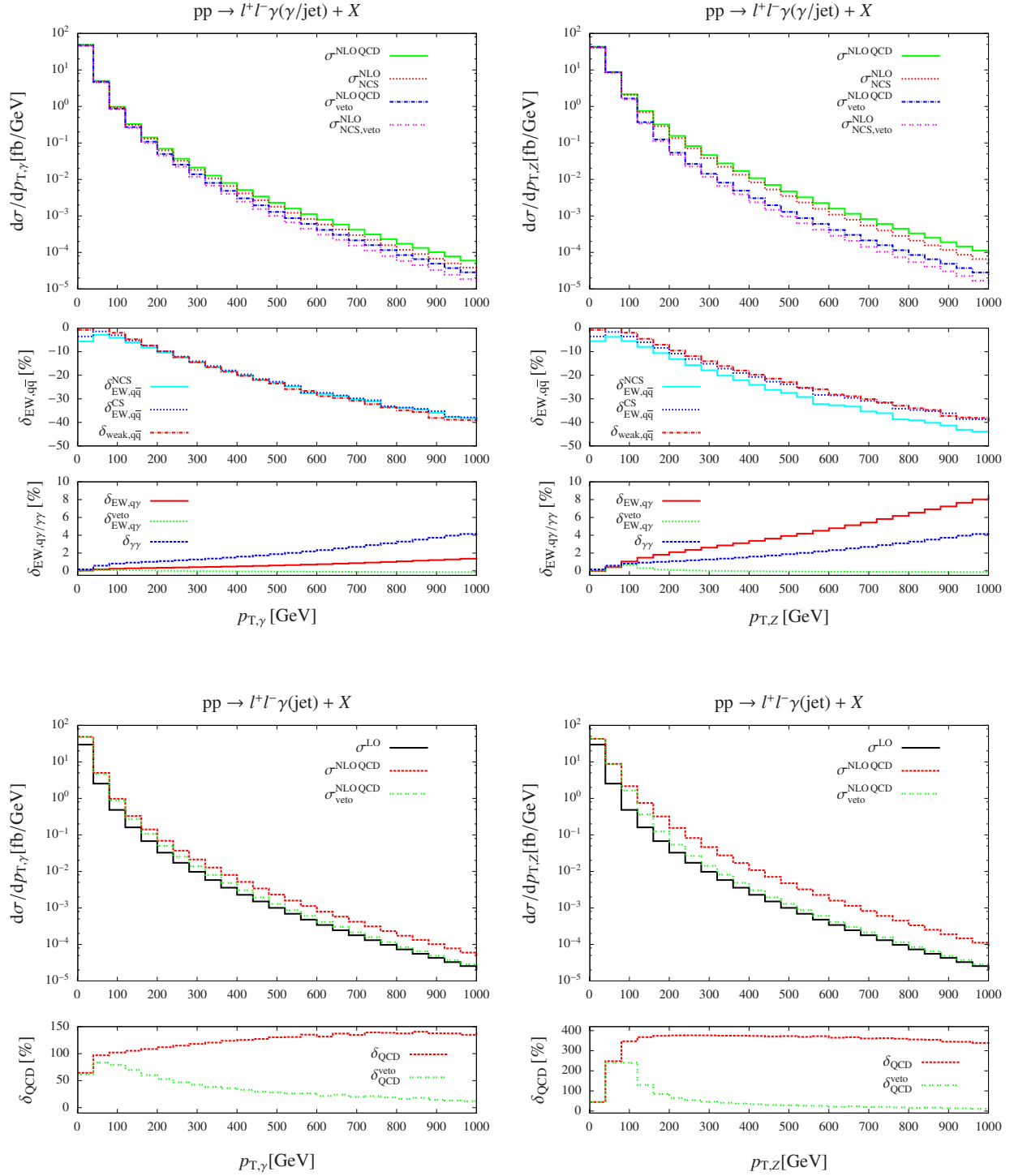


Figure 11: Distributions in the transverse momentum  $p_T$  of the hardest photon (left) and the Z boson (right), including EW (top) and QCD corrections (bottom). The large boxes show absolute predictions, the small ones relative corrections.

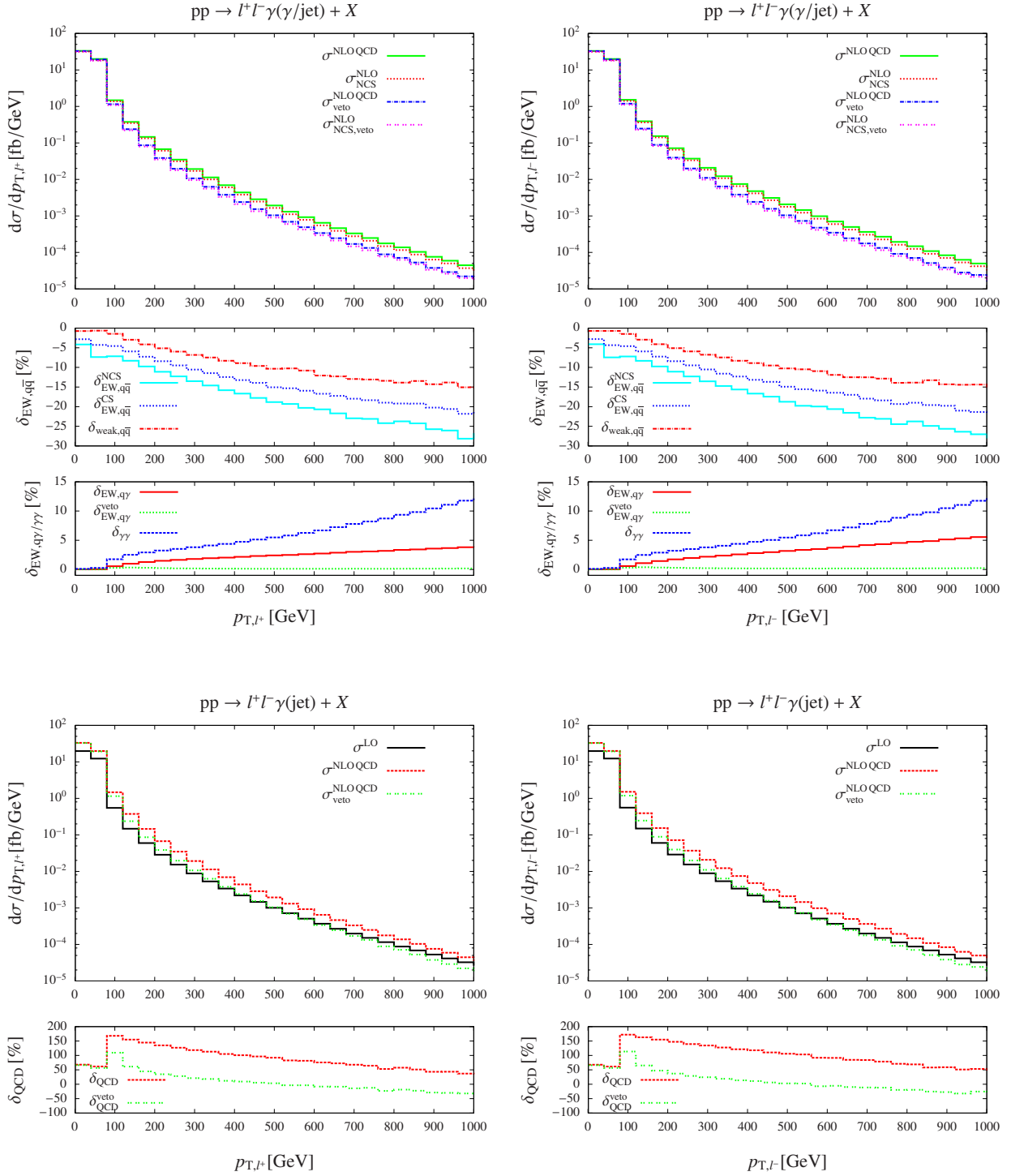


Figure 12: Distributions in the transverse momenta  $p_{T,l^\pm}$  of the two charged leptons, including EW (top) and QCD corrections (bottom). The large boxes show absolute predictions, the small ones relative corrections.



uncertainty for our predictions. It is negligible where the contributions of photon-induced processes are small, but relevant once these get of the order of a percent.

The recipes of the previous two paragraphs can also be used for the following distributions. However, since the corrections are mostly smaller this is also the case for the uncertainties which typically can be considered to be at the level of 1% unless the photonic corrections exceed 1% or the weak corrections exceed 10%.

### 3.3.3 Results on invariant-mass distributions

The invariant mass of the Z boson,  $M_{l+l-}$ , is defined in (3.10), and the invariant three-body mass of the Z-decay products and the photon is defined by

$$M_{l+l-\gamma} = \sqrt{(p_{l+} + p_{l-} + p_{\gamma_1})^2}, \quad (3.12)$$

where  $p_{l+}$ ,  $p_{l-}$ , and  $p_{\gamma_1}$  are the four-vectors of the charged leptons and the hardest photon, respectively. The corresponding distributions are shown in Fig. 13. The invariant-mass distribution of the two charged leptons exhibits two peaks already at LO. The larger one corresponds to the Z resonance originating from the propagator that is resonant in the invariant mass of the two charged leptons  $M_{l+l-}$  at  $M_{l+l-} = M_Z$ . The smaller one comes from the resonance in the invariant three-body mass  $M_{l+l-\gamma}$ , where the photon is radiated by one of the FS charged leptons leading to a shift of the peak. The location of the smaller peak mainly depends on the cut on the transverse momentum of the photon. With decreasing values of the cut on  $p_{T,\gamma}$  the peak becomes less pronounced and moves towards the larger peak until they fuse. The QCD corrections are the leading corrections in this distribution. They are particularly large at low invariant masses and below the resonance with and without a jet veto. This is to some extent a result of our basic cuts, which allow invariant masses  $M_{l+l-}$  down to 40 GeV, but at the same time demand transverse momenta  $p_{T,l^\pm} > 25$  GeV. At LO, this leads to a strong suppression of the cross section at low  $M_{l+l-}$ , but at NLO QCD a jet recoil (with intermediate  $p_{T,\text{jet}} < 100$  GeV) in the real QCD corrections can lift such events over the cuts on  $p_{T,l^\pm}$ , leading to particularly large positive QCD corrections there. In the resonance region the EW corrections coming from the  $q\bar{q}$  channel are strongly dominated by photonic effects and reach 20% in the CS and 40% in the NCS cases. Without photon recombination the shape distortion of the Z resonance is larger, since more events appear where the photon carries away energy and shifts events from higher to lower energies. The purely weak corrections are negligible in the entire range we are looking at. The quark-photon-induced EW corrections are almost zero for low invariant masses and reach 1% at 300 GeV. In case of a jet veto they are well below one percent everywhere. The photon-photon-induced corrections are also tiny for invariant masses below 100 GeV, but grow up to 5% at 300 GeV.

Focusing on the invariant three-body mass we see that the QCD corrections are the dominating contribution in the region of low invariant masses, but decrease with and without a jet veto to 50% and 0%, respectively, for  $M_{l+l-\gamma} = 2$  TeV. In this region, the  $M_{l+l-\gamma}$  distribution receives large negative corrections up to  $-18\%$  from the purely weak contribution, and between  $-23\%$  and  $-28\%$  from the full EW corrections for the CS and the NCS case, respectively. The quark-photon-induced EW corrections are of the order of 1–2% and practically vanish in case of a jet veto, while the photon-photon-induced corrections reach 10% at 2 TeV. At high invariant mass the EW corrections are of the same order of magnitude as the QCD corrections and become the leading corrections in case of a jet veto.

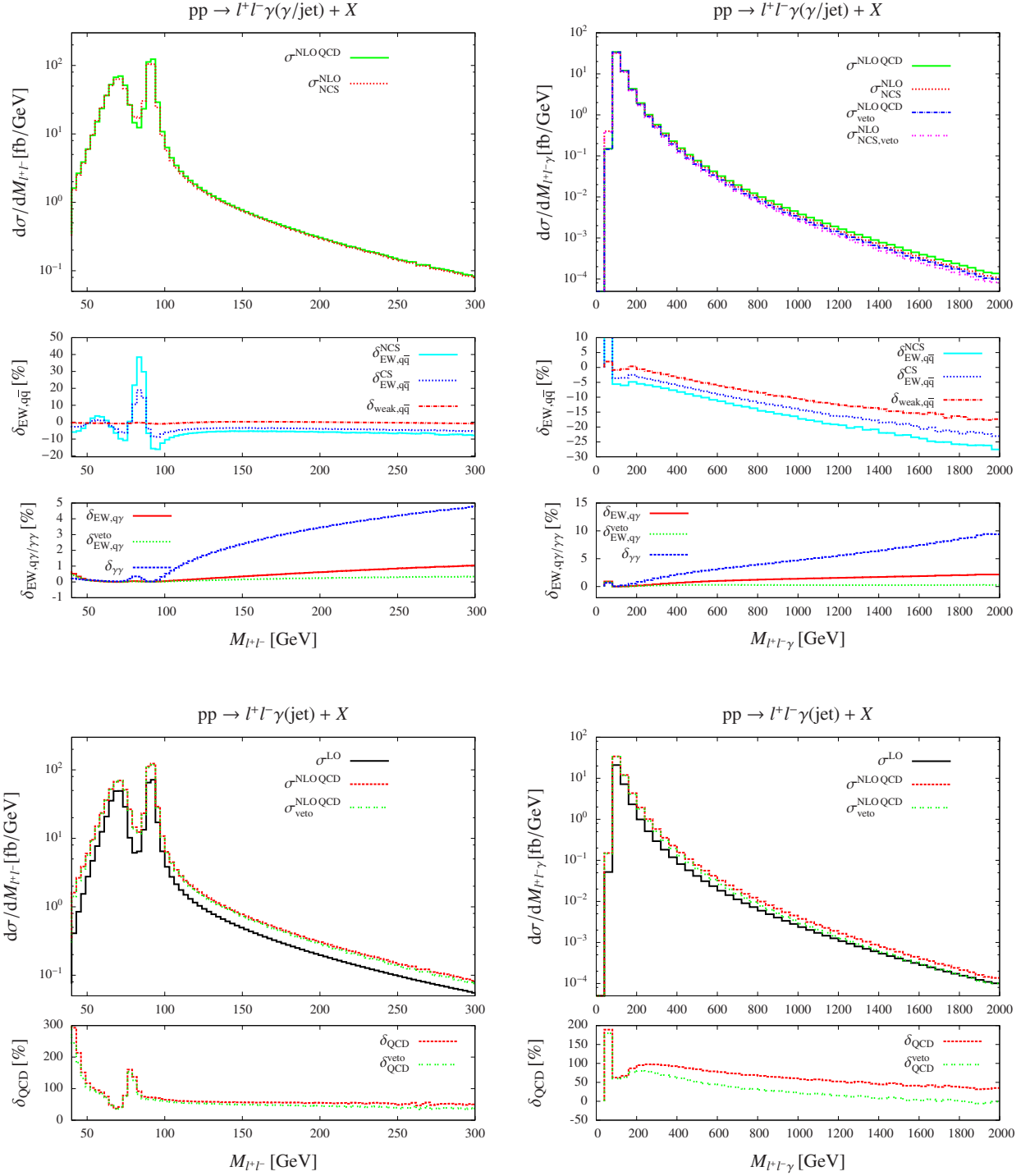


Figure 13: Distribution in the invariant mass  $M_{l+l-}$  of the charged leptons (left) and distribution in the invariant three-body mass  $M_{l+l-\gamma}$  of the charged leptons and the hardest photon (right), including EW (top) and QCD corrections (bottom). The large boxes show absolute predictions, the small ones relative corrections.

### 3.3.4 Results on rapidity and angular distributions

In the following we present some rapidity and angular distributions along with the corresponding NLO corrections. As for the integrated cross section the QCD corrections typically yield the largest contributions and in most cases a jet veto has no sizeable impact. We only show the most interesting distributions and do not single out the purely weak corrections whenever they are negligibly small.

Although the distributions in the rapidity differences  $\Delta y_{\gamma Z}$  and  $\Delta y_{l+\gamma}$  shown in Fig. 14 are different in their absolute values, the relative QCD and EW corrections are very similar in the two cases. The QCD corrections are about 50% at zero rapidity distance and grow to 110% at  $|\Delta y| = 4$ . The quark–antiquark-induced EW corrections amount to roughly  $-3\%$  in the CS case and vary between  $-4\%$  and  $-6\%$  in the NCS case. The photon-induced corrections stay below 1% and are phenomenologically unimportant.

Next we focus on the rapidity difference and the azimuthal-angular difference between the charged leptons shown in Fig. 15. Starting with the rapidity difference we see that the EW corrections to the  $q\bar{q}$  channel have a minimum at zero rapidity difference and increase up to  $-12\%$  and  $-14\%$  at  $|\Delta y_{l+l-}| = 4$  in the CS and the NCS case, respectively. The corrections from the  $q\gamma$  channels are below 4% and 2% with and without a jet veto, respectively. The photon–photon-induced corrections are below 5% for  $|\Delta y_{l+l-}| < 2$  and increase steeply to 30% for  $|\Delta y_{l+l-}| \sim 4$ . However, in this region the cross section is very small.

The azimuthal-angular difference between the charged leptons has a peak around  $160^\circ$ . This peak is caused by the cut on the transverse momentum of the photon which eliminates events with back-to-back leptons in the transverse plane. Increasing this cut shifts the peak to smaller azimuthal angles. The NLO QCD corrections cause a very significant broadening of the peak, because jet recoil effects strongly influence the angle between the leptons when the decaying Z boson receives a boost. The effect is strongest in the limit where the leptons are nearly collinear, a region that is rarely populated at LO, but receives large contributions from hard jet emission where the jet recoil and the boost of the Z boson are strongest. This also explains the sensitivity of this region to the jet veto. The EW corrections from the  $q\bar{q}$  channels are of the order of  $-6\%$  and  $-7\%$  in the CS and the NCS cases, respectively, in the region of small angle differences and decrease at larger ones. In this distribution the weak corrections are of the order of  $-5\%$  at low angles and decrease to the 1% level for angles around the peak. The photon-induced corrections lie below about 1% and are phenomenologically unimportant.

In summary, in angular and rapidity distributions the EW corrections are suppressed with respect to the QCD corrections.

## 3.4 Invisible Z + $\gamma$ production: $pp \rightarrow \bar{\nu}\nu + \gamma + X$

### 3.4.1 Results on total cross sections

In Table 2 we present the LO cross sections  $\sigma^{\text{LO}}$  for different pp centre-of-mass energies  $\sqrt{s}$  and different types of relative corrections  $\delta$  defined in (2.5) for  $pp \rightarrow \bar{\nu}\nu + \gamma + X$ . Recall that we sum over all three lepton generations. Similar to the results in Table 1 we find that the relative corrections only marginally vary for the different collider energies. Here again the QCD corrections give the dominant contributions with  $\sim 40\text{--}50\%$ , about a third to a half of which results from the gluon-induced channels (not separately shown), a much larger share than for  $l^+l^-\gamma$  production. Owing to the neutral final state the dominant contribution inside the quark–antiquark-induced EW corrections results from pure weak corrections with  $\sim -5\%$  and the photonic corrections only contribute 0.3%. Again the quark–photon-induced corrections are phenomenologically negligible.

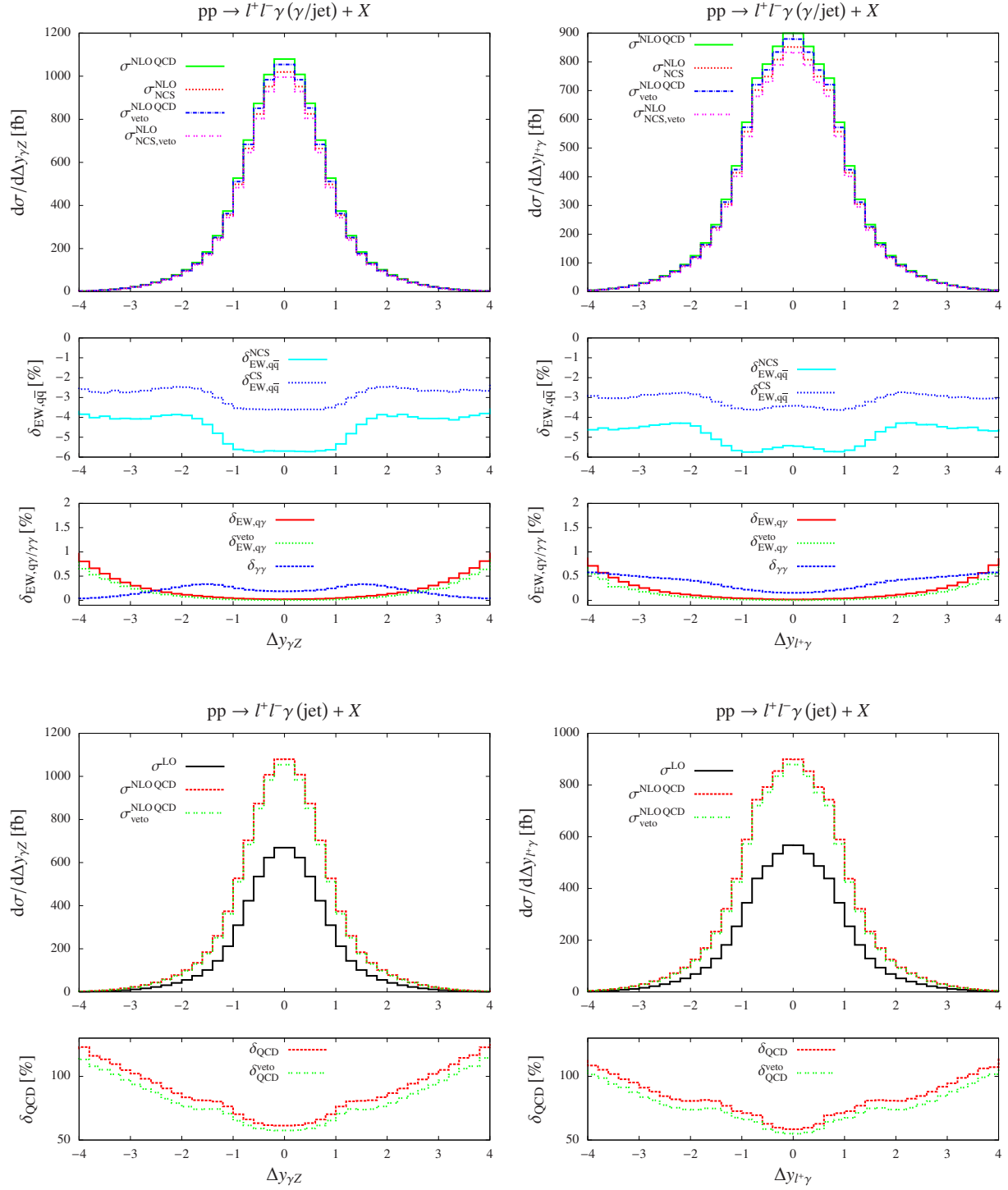


Figure 14: Distributions in the rapidity difference  $\Delta y_{\gamma Z}$  between the hardest photon and the Z boson (left) and the rapidity difference  $\Delta y_{l+\gamma}$  between the charged lepton and the hardest photon (right), including EW (top) and QCD corrections (bottom). The large boxes show absolute predictions, the small ones relative corrections.

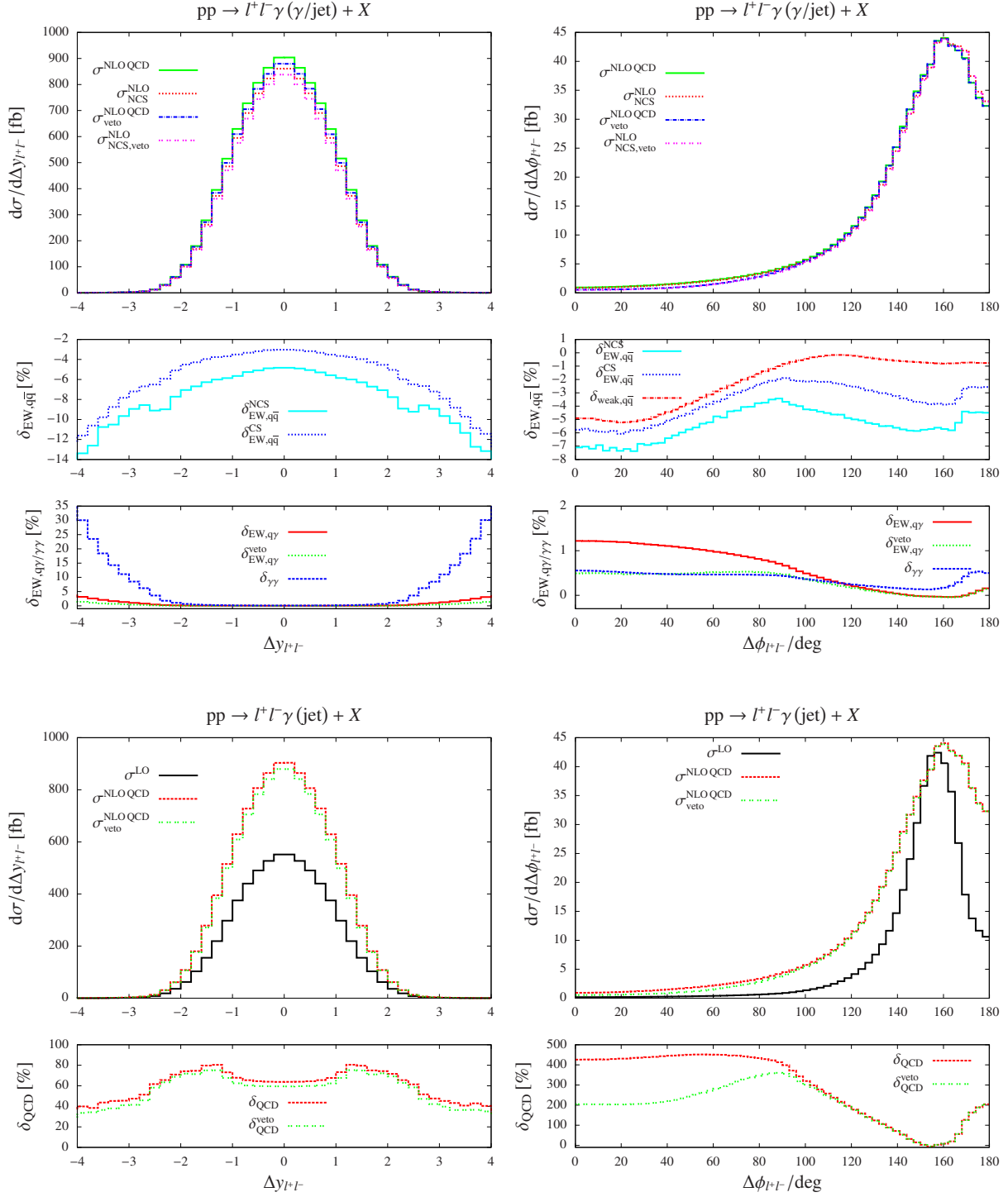


Figure 15: Distributions in the rapidity difference  $\Delta y_{l+l-}$  (left) and the azimuthal-angle difference  $\Delta \phi_{l+l-}$  (right) of the charged leptons, including EW (top) and QCD corrections (bottom). The large boxes show absolute predictions, the small ones relative corrections.

$pp \rightarrow \bar{\nu}\nu\gamma + X$			
$\sqrt{s}/\text{TeV}$	7	8	14
$\sigma^{\text{LO}}/\text{fb}$	74.927(2)	91.031(1)	185.254(4)
$\delta_{\text{phot},q\bar{q}}/\%$	0.30	0.30	0.29(1)
$\delta_{\text{weak},q\bar{q}}/\%$	-4.45	-4.56	-4.98
$\delta_{\text{EW},q\gamma}^{\text{frag}}/\%$	0.03	0.04	0.03
$\delta_{\text{EW},q\gamma}^{\text{veto, frag}}/\%$	0.02	0.03	0.02
$\delta_{\text{EW},q\gamma}^{\text{Frix}}/\%$	0.03	0.03	0.02
$\delta_{\text{EW},q\gamma}^{\text{veto, Frix}}/\%$	0.02	0.02	0.01
$\delta_{\text{QCD}}^{\text{frag}}/\%$	46.35(4)	46.94(5)	51.59(5)
$\delta_{\text{QCD}}^{\text{Frix}}/\%$	45.46(4)	46.07(5)	50.66(3)
$\delta_{\text{QCD}}^{\text{veto, frag}}/\%$	42.57(4)	42.54(3)	44.11(3)
$\delta_{\text{QCD}}^{\text{veto, Frix}}/\%$	41.71(4)	41.67(3)	43.28(3)

Table 2: Integrated cross sections and relative corrections for  $pp \rightarrow \bar{\nu}\nu\gamma + X$  at different LHC energies. The EW corrections to the quark–antiquark annihilation channels are split into purely weak and photonic corrections. Contributions from the photon-induced channels and QCD corrections are shown with a jet veto (veto) as well as without a jet veto using a fragmentation function (frag) or the Frixione isolation criterion (Frix) to separate photons and jets. The numbers in parentheses denote the integration errors in the last digits. This error is omitted if it is negligible at the given accuracy.

### 3.4.2 Results on transverse-momentum distributions

In the following we present differential distributions including QCD and EW corrections to  $pp \rightarrow \bar{\nu}\nu\gamma + X$  for a pp centre-of-mass energy of 14 TeV. In Fig. 16 we show distributions in the transverse momentum of the photon and in the missing transverse momentum. First we notice that the two distributions as well as the corresponding corrections are almost identical. Since the photon neither couples to the Z boson nor to the neutrinos, the photon and the Z boson are always back to back in their centre-of-mass frame at LO. Corrections from the real radiation of jets or photons off the initial-state partons hardly distinguish between the produced Z boson or the hard photon, so that even the NLO corrections (both QCD and EW) almost coincide for the  $p_{T,Z}$  and  $p_{T,\gamma}$  distributions. Furthermore the NLO corrections closely resemble the ones shown in Fig. 11 (left) for the  $p_{T,\gamma}$  distribution for the  $l^+l^-\gamma$  final state. The QCD corrections are similar, because they only affect the IS quarks and do not depend on the final state. The EW corrections corresponding to the  $q\bar{q}$  channel are identical with the weak corrections including the large Sudakov logarithms and turn out to be of similar size quite independent of the final state. The photonic corrections, which only involve the IS quarks, are negligible for  $\bar{\nu}\nu\gamma$  production, i.e. they are almost completely absorbed into the PDFs. The quark–photon-induced corrections roughly differ by a factor of two in the cases of  $l^+l^-\gamma$  and  $\bar{\nu}\nu\gamma$  production, since they depend on the FS particles: In the visible decay channel the IS photon (discussed in Section 3.3) can also couple to the FS charged leptons, whereas in the invisible decay channel it can only couple to the IS quarks.

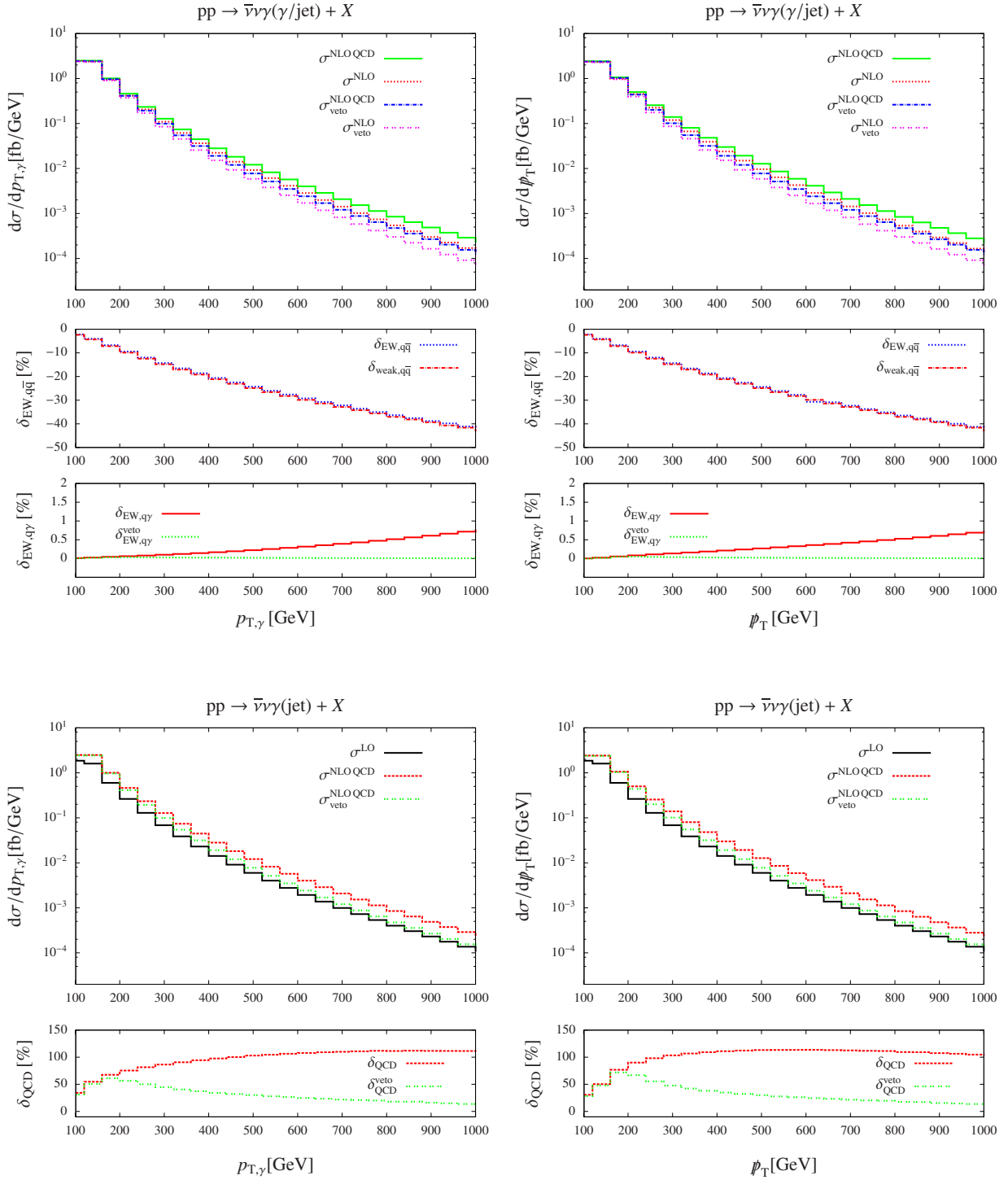


Figure 16: Distributions in the transverse momentum  $p_T$  of the photon (left) and the missing transverse momentum (right), including EW (top) and QCD corrections (bottom). The large boxes show absolute predictions, the small ones relative corrections.

### 3.4.3 Results on transverse-mass distributions

The transverse three-body mass of the neutrinos and the photon is given by

$$M_{T,\bar{\nu}\nu\gamma} = \sqrt{(\not{p}_T + p_{T,\gamma_1})^2 - (\mathbf{p}_T + \mathbf{p}_{T,\gamma_1})^2}, \quad (3.13)$$

where we always take the hardest photon if there are two. The corresponding distribution is shown on the left side of Fig. 17. Comparing this with the invariant three-body mass of the charged leptons and the photon given in Fig. 13, we see that the QCD corrections are flat and have the same trend in both distributions. This can be explained with the same argument as in case of the transverse-momentum distributions, since the QCD corrections only act on the IS quarks and do not depend on the FS leptons. Note that in the invisible decay channel the distribution only starts at 190 GeV at NLO and at 200 GeV at LO owing to the larger  $p_T$  cuts. The EW corrections to the  $q\bar{q}$  channel are considerably larger in the invisible channel which is due to the fact that we consider the *transverse* three-body mass instead of the full three-body mass. If the latter gets large, there is still the possibility that all transverse momenta are moderate or small. By contrast a large transverse three-body mass requires some large transverse momenta, so that the kinematical configuration is closer to the Sudakov regime where all Minkowski products of momenta are large and EW corrections are strongly enhanced. The corrections from the quark-photon channel are below 1% with and without jet veto and therefore negligible.

### 3.4.4 Results on rapidity distributions

The rapidity distribution of the hardest photon is shown on the right side of Fig. 17. It receives large QCD corrections between 30% and 60%. The jet veto diminishes the QCD corrections by 5–10%. The EW corrections to the  $q\bar{q}$  channel mainly originating from the purely weak corrections are of the order of  $-5\%$  and almost flat and therefore reflecting the corrections to the integrated cross section. The EW corrections are small compared to the QCD corrections, but not completely negligible.

## 3.5 Results with anomalous triple gauge-boson couplings

In order to parametrize effects of new physics influencing the non-abelian gauge-boson couplings, higher-dimensional operators can be added to the SM Lagrangian. The commonly used form of anomalous triple gauge-boson couplings (aTGCs) goes back to Ref. [72] and is based on a general parametrization of the WWV, ZZV, and  $Z\gamma V$  vertices (assuming that W and Z bosons couple to conserved currents), with  $V = Z, \gamma$ . In the following we employ the definition of the aTGCs following Refs. [73, 74].

The case of anomalous  $Z\gamma V$  ( $V = Z, \gamma$ ) couplings is particularly interesting, since they do not appear as elementary couplings in the SM. Following Ref. [74], we assume Lorentz and  $U(1)_{\text{em}}$  gauge invariance as well as Bose symmetry. With these assumptions the most general Lagrangian that describes the anomalous VVV vertex is given by

$$\begin{aligned} \mathcal{L}_{VVV} = & \frac{e}{M_Z^2} \left[ -[f_4^\gamma(\partial_\mu F^{\mu\beta}) - f_4^Z(\partial_\mu Z^{\mu\beta})]Z_\alpha(\partial^\alpha Z_\beta) \right. \\ & + [f_5^\gamma(\partial^\sigma F_{\sigma\mu}) - f_5^Z(\partial^\sigma Z_{\sigma\mu})]\tilde{Z}^{\mu\beta}Z_\beta \\ & + [h_1^\gamma(\partial^\sigma F_{\sigma\mu}) - h_1^Z(\partial^\sigma Z_{\sigma\mu})]Z_\beta F^{\mu\beta} + [h_3^\gamma(\partial_\sigma F^{\sigma\rho}) - h_3^Z(\partial_\sigma Z^{\sigma\rho})]Z^\alpha \tilde{F}_{\rho\alpha} \\ & \left. + \left\{ \frac{h_2^\gamma}{M_Z^2}[\partial_\alpha \partial_\beta \partial^\rho F_{\rho\mu}] - \frac{h_2^Z}{M_Z^2}[\partial_\alpha \partial_\beta (\Box + M_Z^2)Z_\mu] \right\} Z^\alpha F^{\mu\beta} \right] \end{aligned}$$



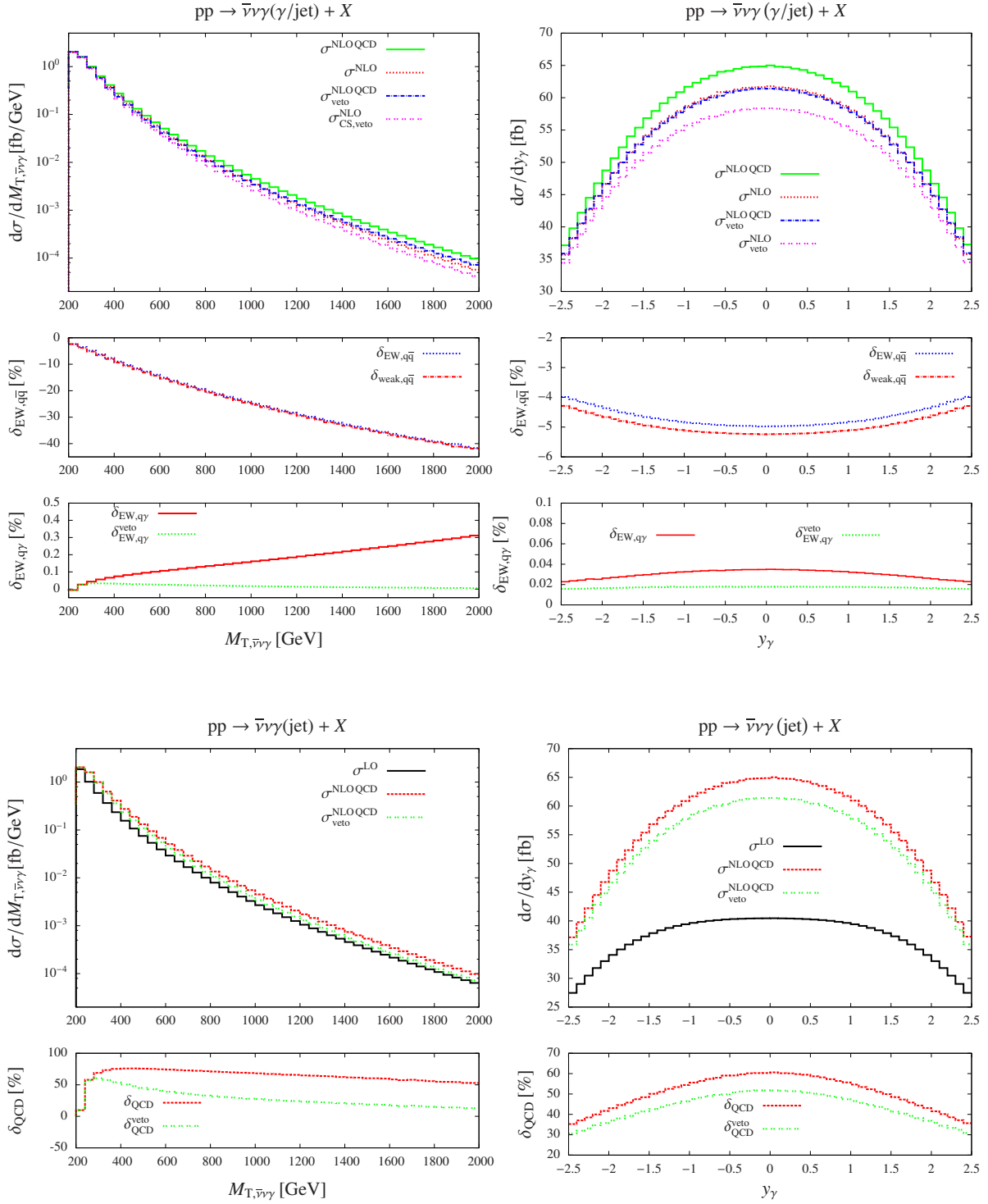


Figure 17: Distributions in the transverse three-body mass  $M_{T,\bar{\nu}\nu\gamma}$  of the neutrino pair and the hardest photon and in the rapidity  $y_\gamma$  of the hardest photon, including EW (top) and QCD corrections (bottom). The large boxes show absolute predictions, the small ones relative corrections.

$$- \left\{ \frac{h_4^\gamma}{2M_Z^2} [\square \partial^\sigma F^{\rho\alpha}] - \frac{h_4^Z}{2M_Z^2} [(\square + M_Z^2) \partial^\sigma Z^{\rho\alpha}] \right\} Z_\sigma \tilde{F}_{\rho\alpha} \Big], \quad (3.14)$$

where  $Z^\mu$  is the Z-boson field,  $Z^{\mu\nu} = \partial^\mu Z^\nu - \partial^\nu Z^\mu$ ,  $\tilde{Z}_{\mu\nu} = \epsilon_{\mu\nu\rho\sigma} Z^{\rho\sigma}/2$ , and  $\tilde{F}_{\mu\nu} = \epsilon_{\mu\nu\rho\sigma} F^{\rho\sigma}/2$ . The anomalous couplings proportional to  $f_4^V$ ,  $h_1^V$ ,  $h_2^V$  violate CP symmetry whereas the ones proportional to  $f_5^V$ ,  $h_3^V$ ,  $h_4^V$  respect it. Note that our conventions for the SM Lagrangian taken from Ref. [75] differ from those of Ref. [74] by a minus sign in the Z-boson and other fields not appearing in Eq. (3.14), a difference that uniformly applies to SM and non-standard couplings. The operators in Eq. (3.14) exploit all possible Lorentz structures that do not include the scalar components of any of the two vector bosons, i.e. the Lagrangian assumes that

$$\partial_\mu A^\mu = 0, \quad \partial_\mu Z^\mu = 0. \quad (3.15)$$

This relation also effectively holds for virtual photons and Z bosons in our case, since terms containing  $\partial Z$  lead to contributions to amplitudes that are proportional to the lepton or quark masses, which are neglected, because the Z boson couples to a conserved current in the limit of small fermion masses. With the Lagrangian (3.14) the momentum-space Feynman rules for the anomalous ZZ $\gamma$  and Z $\gamma\gamma$  vertices read

$$\begin{aligned} \Gamma_{ZZ\gamma}^{\mu\nu\alpha}(Q, q, k) = & - \frac{ie}{M_Z^2} (Q^2 - q^2) \left\{ h_1^Z (k^\mu g^{\nu\alpha} - k^\nu g^{\mu\alpha}) - h_3^Z \epsilon^{\mu\nu\alpha\beta} k_\beta \right\} \\ & - \frac{ie}{M_Z^2} (Q^2 - M_Z^2) \left\{ \frac{h_2^Z}{M_Z^2} Q^\nu [(k \cdot Q) g^{\mu\alpha} - k^\mu Q^\alpha] - \frac{h_4^Z}{M_Z^2} Q^\nu \epsilon^{\mu\alpha\beta\delta} Q_\beta k_\delta \right\} \\ & - \frac{ie}{M_Z^2} (q^2 - M_Z^2) \left\{ \frac{h_2^Z}{M_Z^2} q^\nu [(k \cdot q) g^{\nu\alpha} - k^\nu Q^\alpha] - \frac{h_4^Z}{M_Z^2} q^\mu \epsilon^{\nu\alpha\beta\delta} q_\beta k_\delta \right\} + \dots, \end{aligned} \quad (3.16)$$

$$\begin{aligned} \Gamma_{Z\gamma\gamma}^{\mu\nu\alpha}(Q, q, k) = & \frac{ie}{M_Z^2} q^2 \left\{ - h_1^\gamma (k^\mu g^{\nu\alpha} - k^\nu g^{\mu\alpha}) + h_3^\gamma \epsilon^{\mu\nu\alpha\beta} k_\beta \right. \\ & \left. + \frac{h_2^\gamma}{M_Z^2} q^\mu [(k \cdot q) g^{\nu\alpha} - k^\nu q^\alpha] - \frac{h_4^\gamma}{M_Z^2} q^\mu \epsilon^{\nu\alpha\delta\rho} q_\delta k_\rho \right\} + \dots, \end{aligned} \quad (3.17)$$

where all momenta are considered as incoming and all terms are omitted that do not contribute for an on-shell photon with momentum  $k$ . Assuming that one Z boson is approximately on shell ( $q^2 \sim M_Z^2$ ), we find the same vertex as derived in Refs. [23, 74].

The anomalous couplings spoil unitarity of the S-matrix in the limit of high energies. This behaviour is usually tamed by including form factors, mimicking the onset of new physics that damps the effects of the aTGCs at high momentum transfer. We use the standard form factors

$$h_i^V \rightarrow \frac{h_i^V}{\left(1 + \frac{M_{Z\gamma}^2}{\Lambda^2}\right)^n}, \quad (3.18)$$

where  $V = \gamma, Z$ , the scale of new physics is denoted as  $\Lambda$ , and  $M_{Z\gamma}$  is the invariant mass of the Z-boson-photon system. The exponent  $n$  is chosen such that the form factor decreases fast enough to restore unitarity.

In order to combine the contribution of the anomalous couplings (AC) with the NLO corrections in a consistent way, we extend Eq. (2.4) by the relative anomalous contribution  $\delta_{AC}$ ,

$$\sigma_{AC}^{\text{NLO}} = \sigma^{\text{NLO QCD}} (1 + \delta_{EW, q\bar{q}} + \delta_{AC}) + \Delta\sigma_{q\gamma}^{\text{NLO EW}} + (\Delta\sigma_{\gamma\gamma}^{\text{NLO EW}}), \quad (3.19)$$

where  $\delta_{\text{AC}}$  is defined by

$$\delta_{\text{AC}} = \frac{\sigma_{\text{AC}}^{\text{NLO QCD}}}{\sigma^{\text{NLO QCD}}} - 1. \quad (3.20)$$

The SM cross section  $\sigma^{\text{NLO QCD}}$  is defined in Sect. 2.1, and  $\sigma_{\text{AC}}^{\text{NLO QCD}}$  is the NLO QCD cross section including the aTGC contribution. Thus,  $\delta_{\text{AC}}$  can be considered as an additional correction on top of the EW correction in (2.4) which we choose to combine linearly. A proper combination of aTGCs and EW corrections would require an effective-field-theory approach, which goes beyond the scope of this work. In contrast, QCD corrections can be calculated in a straightforward way in the presence of aTGCs.

For our calculation we choose values for the ACs consistent with the most recent limits set by the ATLAS and CMS collaborations in Refs. [7, 10]. Following these references we demand CP conservation which is equivalent to  $h_{1,2}^V = 0$ . In Refs. [7, 10] limits were set on the remaining ACs for two different scales that enter the form factor defined in Eq. (3.18). We choose the following two sets of values,

$$\begin{aligned} \Lambda = 3 \text{ TeV} : \quad & h_3^\gamma = 2.4 \cdot 10^{-2}, \quad h_4^\gamma = 3.6 \cdot 10^{-4}, \quad h_3^Z = 2.0 \cdot 10^{-2}, \quad h_4^Z = 3.1 \cdot 10^{-4}; \\ \Lambda \rightarrow \infty : \quad & h_3^\gamma = 4.6 \cdot 10^{-3}, \quad h_4^\gamma = 3.5 \cdot 10^{-5}, \quad h_3^Z = 3.7 \cdot 10^{-3}, \quad h_4^Z = 3.0 \cdot 10^{-5}. \end{aligned} \quad (3.21)$$

The former numbers for  $\Lambda = 3 \text{ TeV}$  reflect the limits set by ATLAS [7] using data from the run at an energy of 7 TeV with a luminosity of  $4.6 \text{ fb}^{-1}$ , the latter values without form factor ( $\Lambda \rightarrow \infty$ ) correspond to the limits set by CMS [10] after collecting a luminosity of  $19.5 \text{ fb}^{-1}$  at 8 TeV. Following Ref. [23] we choose the exponent of the form factor as  $n = 3$  and  $n = 4$  for the ACs  $h_3^V$  and  $h_4^V$ , respectively.

Analyzing the impact of aTGCs for  $\sqrt{s} = 14 \text{ TeV}$  we only present results obtained without a jet veto, since the impact of a jet veto does not change the effect of the ACs significantly. Note that we only present QCD-corrected distributions in the following. Therefore we do not have to distinguish between the CS and the NCS cases.

### 3.5.1 $pp \rightarrow l^+ l^- + \gamma + X$

In Fig. 18 we analyse the impact of aTGCs on the transverse-momentum distributions of the photon and the charged lepton corresponding to the visible decay channel of the Z boson. Focusing on the  $p_{\text{T},\gamma}$  distribution we see that the aTGCs start to cause a visible effect roughly at 200 GeV and at 350 GeV in case of  $\Lambda = 3 \text{ TeV}$  and  $\Lambda \rightarrow \infty$ , respectively. The relative contributions of the aTGCs meet at 450 GeV and develop in the same way staying almost constant. The relative corrections are huge growing up to  $10^3$  at 1 TeV. The situation is different in the  $p_{\text{T},l^+}$  distribution. Here the contributions of the aTGCs from the two setups overlap at small transverse momenta and start to have a visible effect around 150 GeV. At higher transverse momenta they diverge, where the contribution without form factor remains almost constant, whereas the contribution with form factor decreases. The relative impact coming from the aTGCs reach a factor of  $10^4$  at 1 TeV. For a fixed set of AC values, one of course would expect larger aTGC effects for the case without form factor  $\Lambda \rightarrow \infty$ , since a finite form factor effectively switches off the AC contribution at high energies. Recall, however, that our AC values chosen for  $\Lambda \rightarrow \infty$  correspond to limits set in a fit to data collected at a somewhat higher pp energy with a significantly higher luminosity, so that at least for the formerly experimentally accessible energy scales in the distributions the impact of the

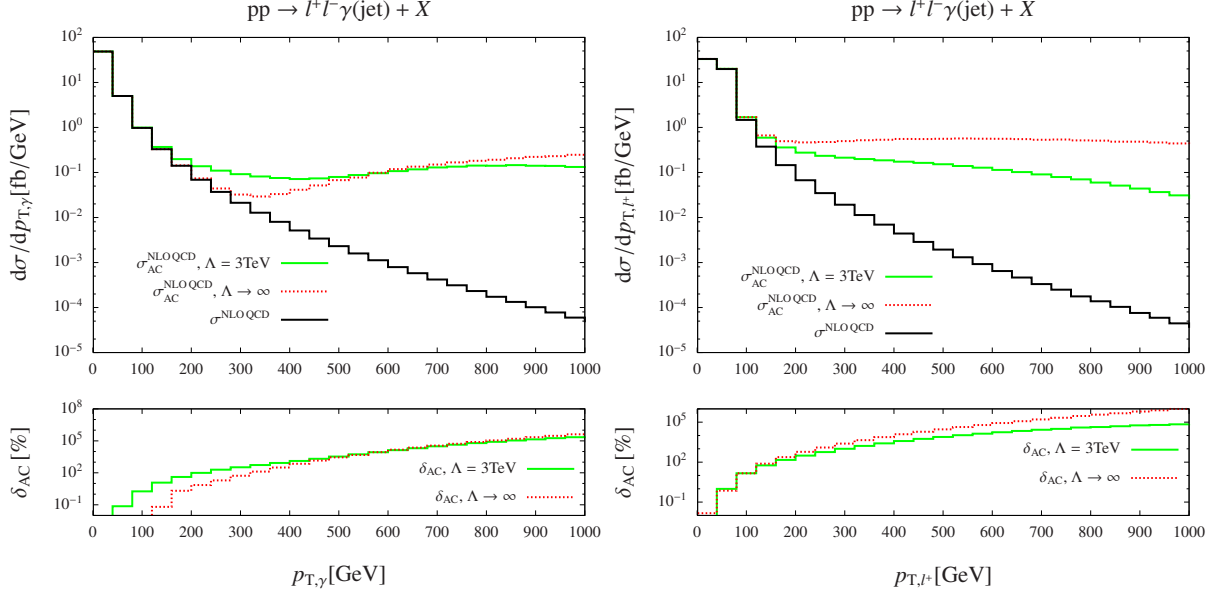


Figure 18: Absolute and relative contributions of aTGCs to the transverse-momentum distributions of the photon (left) and the charged lepton (right).

ACs with  $\Lambda \rightarrow \infty$  is expected to be somewhat smaller than for the set of AC values with  $\Lambda = 3$  TeV. This behaviour is, for instance, found in the  $p_{T,\gamma}$  distribution in Fig. 18.

Next we analyse the invariant mass of the charged leptons and the invariant three-body mass of the charged leptons and the photon shown in Fig. 19. Starting with the  $M_{l+l-}$  distribution we see that the aTGCs only have a significant impact on the invariant-mass distribution around the Z pole. At higher invariant masses up to several 100 GeV the aTGCs have almost no effect. This can be explained exactly in the same way as in the case of  $W + \gamma$  production, where amongst others we analysed the impact of aTGCs on the transverse-mass distribution of the charged lepton and the neutrino in Ref. [40]. At large invariant mass  $M_{l+l-}$  the intermediate bosons Z and V coupled to the anomalous  $V\gamma Z$  ( $V = \gamma, Z$ ) vertex are far off shell. This fact allows us to explain the small effect of aTGCs at large invariant masses, which are typically driven by disturbing the unitarity cancellations of the SM amplitude. In case of resonant Z bosons these cancellations occur for longitudinally polarized Z bosons with momentum  $q^\mu$  and virtuality  $q^2 \sim M_Z^2$ , where the effective Z polarization vector behaves like  $\varepsilon_L^\mu \sim q^\mu / \sqrt{q^2} \sim q^\mu / M_Z$ . For large invariant masses, the Z virtuality is large,  $q^2 \gg M_Z^2$ , so that  $\varepsilon_L^\mu \sim q^\mu / \sqrt{q^2}$  is suppressed, and no large cancellations are necessary within the amplitude to avoid unitarity violations in the SM. The suppression in the polarization  $\varepsilon_L^\mu$  explains why there is no effect of the aTGCs visible in the high-mass tail of the invariant-mass distribution in contrast to other scale-dependent distributions. The impact of aTGCs near the Z pole is much higher for the case without form factor in comparison to the setup with  $\Lambda = 3$  TeV, although the AC values for  $\Lambda \rightarrow \infty$  are much smaller. The arguments given above for the transverse-momentum distributions, which lead to the expectation that the AC effects for  $\Lambda \rightarrow \infty$  should be smaller, do not apply here, because the aTGC effects without form factor are dominated by extremely large scattering energies even for  $M_{l+l-} \sim M_Z$ . Here, it should be kept in mind that the limits (3.21) were obtained for LHC energies of 7/8 TeV, but our results are for an energy of 14 TeV.

In Fig. 19 (right) we observe a large impact of the aTGCs on the distribution in the invariant three-body mass. The relative corrections from the aTGCs obtained with and without a form factor

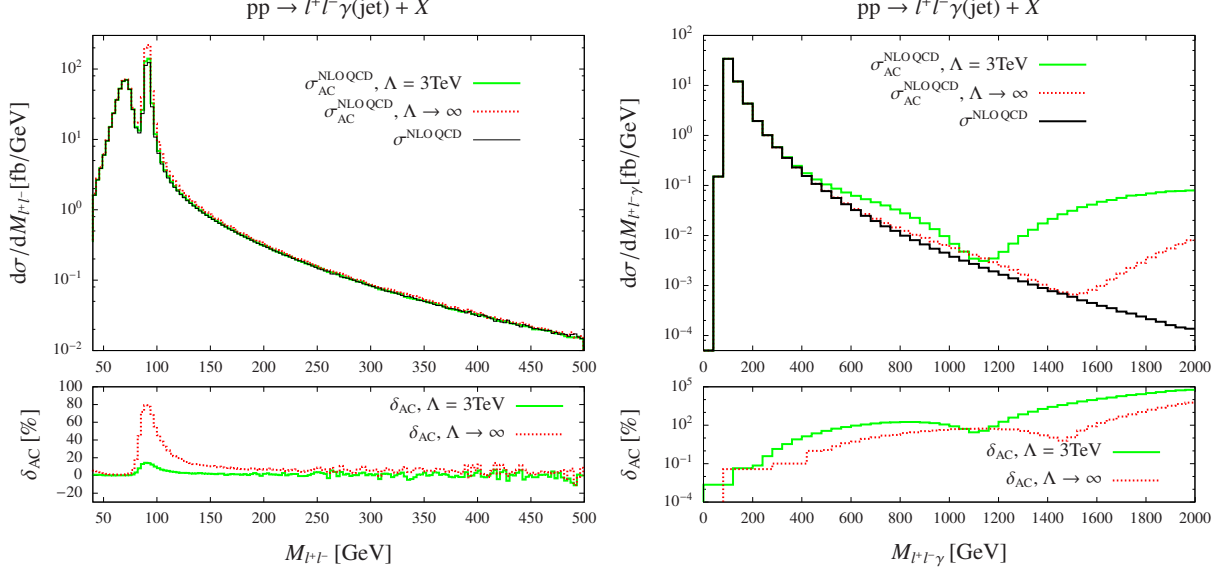


Figure 19: Absolute and relative contributions of aTGCs to the invariant-mass distribution of the charged leptons (left) and to the invariant three-body mass of the charged leptons and the hardest photon (right).

grow to  $10^3$  and  $10^2$  at 2 TeV, respectively. With the same arguments as before we can now explain why the effect of the aTGCs is so large here. A high invariant three-body mass can occur while the outgoing Z boson is on shell if the outgoing photon carries away a sufficiently large amount of the energy brought into the  $V\gamma Z$  vertex ( $V = \gamma, Z$ ) by the incoming boson. Therefore the longitudinal polarization vector of the outgoing Z boson, which is effectively produced by the leptonic decay current, is not suppressed leading to a large contribution of the aTGCs at high invariant three-body masses. In view of the hierarchy of the impact of aTGCs in our two setups, the arguments given for the transverse-momentum spectra again apply, i.e. the case without form factor shows a smaller AC impact up to moderate scales, because the corresponding set of AC values is stronger constrained by data in this range.

### 3.5.2 $pp \rightarrow \bar{\nu}\nu\gamma + X$

Turning to the invisible decay channel of the Z boson we show the transverse-momentum distribution of the photon and the transverse three-body mass of the neutrinos and the photon in Fig. 20. The  $p_T$  distribution of the photon receives the same corrections from aTGCs as the  $p_T$  distribution of the photon in case of the visible decay channel of the Z boson. This is due to the fact that the cross-section contributions by aTGCs do not depend on the FS particles. In case of the *transverse* three-body mass distribution the relative contribution of the aTGCs increases much faster than in the  $M_{l^+l^-\gamma}$  distribution, which is again due to the influence of events where the three-body invariant mass is much higher than the transverse three-body mass. Since aTGC contributions grow with higher invariant masses, the relative contribution of the aTGCs increases faster in case of the transverse three-body mass.

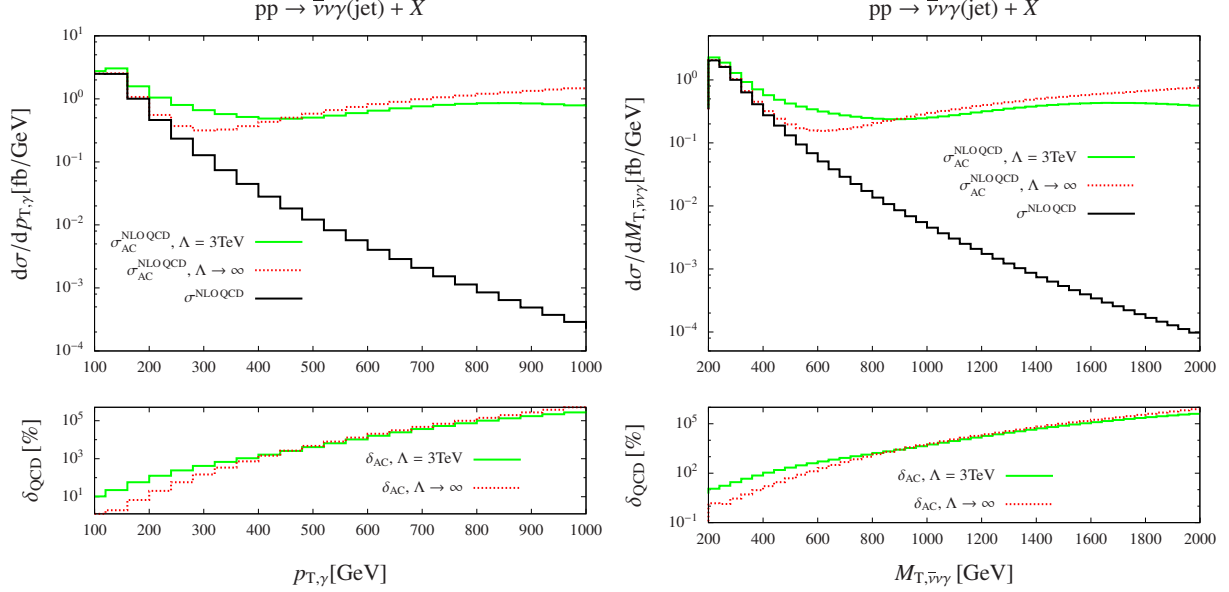


Figure 20: Absolute and relative contributions of aTGCs to the transverse-momentum distribution of the photon (left) and to the transverse three-body mass of the neutrinos and the hardest photon (right).

## 4 Conclusions

Analyzing  $Z + \gamma$  final states at hadron colliders offers several directions to probe the SM and to look for traces of new physics. Final states with charged leptons,  $l^+l^-\gamma$ , are ideal to look for non-standard effects in  $ZZ\gamma$  and  $Z\gamma\gamma$  couplings, which do not exist in the SM as elementary interactions. On the other hand, final states with invisibly decaying Z bosons and a hard photon, known as mono-photon production, are prominent signatures of many exotic new-physics models. Both types of reactions require improved theoretical predictions for experimental analyses at run 2 of the LHC.

In this paper we have improved the knowledge of  $Z + \gamma$  production on the side of electroweak higher-order corrections for both process types. Specifically, we have calculated the full next-to-leading-order electroweak corrections to the processes  $pp \rightarrow l^+l^-/\bar{\nu}\nu + \gamma + X$ , taking into account all off-shell effects of the Z boson using the complex-mass scheme and including all partonic channels ( $q\gamma$  and  $\gamma\gamma$ ) with initial-state photons. In order to discuss the phenomenological separation of  $Z + \gamma$  or  $Z + \text{jet}$  production, we have recalculated the NLO QCD corrections. The actual distinction between hard photons and hard jets in their overlap region is performed in two alternative ways by employing a quark-to-photon fragmentation function or Frixione's cone isolation.

Reflecting the known general feature of EW corrections in the TeV range, we find those corrections of the size of several 10% in distributions, while their impact on integrated cross sections remains at the level of some percent. The impact of photon-induced channels is moderate or small throughout, reaching some percent in extreme regions of distributions.

We estimate the theoretical uncertainties from missing higher-order electroweak corrections to be of the order of 0.5% for integrated cross sections and 1% for differential distributions. For distributions, where the contributions from photon-induced channels exceed one percent these contributions should be viewed as an additional theoretical uncertainty. Moreover, if electroweak corrections surpass 10% their square should be considered as a measure for the missing electroweak corrections beyond next-to-leading order.

On top of our complete NLO EW+QCD predictions in the SM, we have included non-standard effects in  $ZZ\gamma$  and  $Z\gamma\gamma$  couplings at the NLO QCD level in the usual approach of anomalous couplings, on which previous Tevatron and LHC analyses were based. In view of future global analyses of non-standard couplings in the effective field theory approach with dimension-six operators, also the  $Z + \gamma$  analyses should be performed in this framework. On the theoretical side this task is straightforward at the NLO QCD level, but delicate if EW corrections should be combined with non-standard operators beyond a mere addition. These issue is left to future work.

Within the SM, our calculations constitute an important part of state-of-the-art predictions for  $Z + \gamma$  production. To this end, our results should be combined with the recently published next-to-next-to-leading-order QCD predictions, e.g. upon including differential reweighting factors for the EW corrections on top of the absolute QCD predictions. This combination should provide the necessary precision in predictions required for the coming data analysis at the LHC at its design energy and luminosity.

## Acknowledgements

The work of S.D. and M.H. is supported by the German Research Foundation (DFG) via grant DI 784/2-1 and the Research Training Group GRK 1102 “Physics at Hadron Colliders”. The work of A.D. and C.P. is supported by the Research Training Group GRK 1147 “Theoretical Astrophysics and Particle Physics”.

## References

- [1] A. Djouadi, M. Spira, and P. M. Zerwas, Phys. Lett. **B264** (1991) 440.
- [2] S. Dawson, Nucl. Phys. **B359** (1991) 283.
- [3] M. Spira, A. Djouadi, D. Graudenz, and P. M. Zerwas, Nucl. Phys. **B453** (1995) 17, [arXiv:hep-ph/9504378 \[hep-ph\]](#).
- [4] A. Djouadi, V. Driesen, W. Hollik, and A. Kraft, Eur. Phys. J. **C1** (1998) 163, [arXiv:hep-ph/9701342 \[hep-ph\]](#).
- [5] CDF, T. Aaltonen *et al.*, Phys. Rev. Lett. **107** (2011) 051802, [arXiv:1103.2990 \[hep-ex\]](#).
- [6] D0, V. M. Abazov *et al.*, Phys. Rev. **D85** (2012) 052001, [arXiv:1111.3684 \[hep-ex\]](#).
- [7] ATLAS, G. Aad *et al.*, Phys.Rev. **D87** (2013) 11, 112003, [arXiv:1302.1283 \[hep-ex\]](#).
- [8] ATLAS, G. Aad *et al.*, Phys.Lett. **B738** (2014) 428, [arXiv:1407.8150 \[hep-ex\]](#).
- [9] CMS, S. Chatrchyan *et al.*, Phys.Rev. **D89** (2014) 092005, [arXiv:1308.6832 \[hep-ex\]](#).
- [10] CMS, V. Khachatryan *et al.*, JHEP **04** (2015) 164, [arXiv:1502.05664 \[hep-ex\]](#).
- [11] P. J. Fox, R. Harnik, J. Kopp, and Y. Tsai, Phys. Rev. **D85** (2012) 056011, [arXiv:1109.4398 \[hep-ph\]](#).
- [12] G. Belanger, M. Heikinheimo, and V. Sanz, JHEP **08** (2012) 151, [arXiv:1205.1463 \[hep-ph\]](#).

- [13] E. Gabrielli, M. Heikinheimo, B. Mele, and M. Raidal, Phys. Rev. **D90** (2014) 5, 055032, [arXiv:1405.5196 \[hep-ph\]](#).
- [14] F. Maltoni, A. Martini, K. Mawatari, and B. Oehl, JHEP **04** (2015) 021, [arXiv:1502.01637 \[hep-ph\]](#).
- [15] CDF, T. Aaltonen *et al.*, Phys. Rev. Lett. **101** (2008) 181602, [arXiv:0807.3132 \[hep-ex\]](#).
- [16] D0, V. M. Abazov *et al.*, Phys. Rev. Lett. **101** (2008) 011601, [arXiv:0803.2137 \[hep-ex\]](#).
- [17] ATLAS, G. Aad *et al.*, Phys. Rev. **D91** (2015) 1, 012008, [arXiv:1411.1559 \[hep-ex\]](#).  
[Erratum: Phys. Rev.D92,no.5,059903(2015)].
- [18] CMS, V. Khachatryan *et al.*, [arXiv:1410.8812 \[hep-ex\]](#).
- [19] F. M. Renard, Nucl. Phys. **B196** (1982) 93.
- [20] J. Ohnemus, Phys.Rev. **D47** (1993) 940.
- [21] J. Ohnemus, Phys. Rev. **D51** (1995) 1068, [arXiv:hep-ph/9407370 \[hep-ph\]](#).
- [22] U. Baur, T. Han, and J. Ohnemus, Phys. Rev. **D57** (1998) 2823, [arXiv:hep-ph/9710416 \[hep-ph\]](#).
- [23] D. De Florian and A. Signer, Eur.Phys.J. **C16** (2000) 105, [arXiv:hep-ph/0002138 \[hep-ph\]](#).
- [24] L. J. Dixon, Z. Kunszt, and A. Signer, Nucl.Phys. **B531** (1998) 3, [arXiv:hep-ph/9803250 \[hep-ph\]](#).
- [25] J. M. Campbell, R. K. Ellis, and C. Williams, JHEP **1107** (2011) 018, [arXiv:1105.0020 \[hep-ph\]](#).
- [26] M. Grazzini, S. Kallweit, D. Rathlev, and A. Torre, Phys. Lett. **B731** (2014) 204, [arXiv:1309.7000 \[hep-ph\]](#).
- [27] M. Grazzini, S. Kallweit, and D. Rathlev, JHEP **07** (2015) 085, [arXiv:1504.01330 \[hep-ph\]](#).
- [28] J. J. van der Bij and E. W. N. Glover, Phys. Lett. **B206** (1988) 701.
- [29] W. Beenakker, A. Denner, S. Dittmaier, R. Mertig, and T. Sack, Nucl.Phys. **B410** (1993) 245.
- [30] M. Beccaria, G. Montagna, F. Piccinini, F. Renard, and C. Verzegnassi, Phys.Rev. **D58** (1998) 093014, [arXiv:hep-ph/9805250 \[hep-ph\]](#).
- [31] P. Ciafaloni and D. Comelli, Phys.Lett. **B446** (1999) 278, [arXiv:hep-ph/9809321 \[hep-ph\]](#).
- [32] J. H. Kühn and A. Penin, [arXiv:hep-ph/9906545 \[hep-ph\]](#).
- [33] V. S. Fadin, L. N. Lipatov, A. D. Martin, and M. Melles, Phys. Rev. **D61** (2000) 094002, [arXiv:hep-ph/9910338 \[hep-ph\]](#).



- [34] A. Denner and S. Pozzorini, Eur.Phys.J. **C18** (2001) 461, [arXiv:hep-ph/0010201 \[hep-ph\]](#).
- [35] W. Hollik and C. Meier, Phys. Lett. **B590** (2004) 69, [arXiv:hep-ph/0402281 \[hep-ph\]](#).
- [36] E. Accomando, A. Denner, and C. Meier, Eur.Phys.J. **C47** (2006) 125, [arXiv:hep-ph/0509234 \[hep-ph\]](#).
- [37] E. W. N. Glover and A. G. Morgan, Z. Phys. **C62** (1994) 311.
- [38] E. W. N. Glover and A. G. Morgan, Phys. Lett. **B334** (1994) 208.
- [39] S. Frixione, Phys.Lett. **B429** (1998) 369, [arXiv:hep-ph/9801442 \[hep-ph\]](#).
- [40] A. Denner, S. Dittmaier, M. Hecht, and C. Pasold, JHEP **04** (2015) 018, [arXiv:1412.7421 \[hep-ph\]](#).
- [41] S. Dittmaier, Phys.Rev. **D59** (1998) 016007, [arXiv:hep-ph/9805445 \[hep-ph\]](#).
- [42] A. Denner, S. Dittmaier, and L. Hofer, PoS **LL2014** (2014) 071, [arXiv:1407.0087 \[hep-ph\]](#).
- [43] A. Denner and S. Dittmaier, Nucl.Phys. **B658** (2003) 175, [arXiv:hep-ph/0212259 \[hep-ph\]](#).
- [44] A. Denner and S. Dittmaier, Nucl.Phys. **B734** (2006) 62, [arXiv:hep-ph/0509141 \[hep-ph\]](#).
- [45] A. Denner and S. Dittmaier, Nucl.Phys. **B844** (2011) 199, [arXiv:1005.2076 \[hep-ph\]](#).
- [46] T. Hahn, Comput.Phys.Commun. **140** (2001) 418, [arXiv:hep-ph/0012260 \[hep-ph\]](#).
- [47] T. Hahn and C. Schappacher, Comput.Phys.Commun. **143** (2002) 54, [arXiv:hep-ph/0105349 \[hep-ph\]](#).
- [48] T. Hahn and M. Perez-Victoria, Comput.Phys.Commun. **118** (1999) 153, [arXiv:hep-ph/9807565 \[hep-ph\]](#).
- [49] E. Accomando, A. Denner, and S. Pozzorini, Phys.Rev. **D65** (2002) 073003, [arXiv:hep-ph/0110114 \[hep-ph\]](#).
- [50] J. Küblbeck, M. Böhm, and A. Denner, Comput.Phys.Commun. **60** (1990) 165.
- [51] S. Dittmaier, Nucl.Phys. **B565** (2000) 69, [arXiv:hep-ph/9904440 \[hep-ph\]](#).
- [52] S. Dittmaier, A. Kabelschacht, and T. Kasprzik, Nucl.Phys. **B800** (2008) 146, [arXiv:0802.1405 \[hep-ph\]](#).
- [53] S. Catani and M. H. Seymour, Nucl. Phys. **B485** (1997) 291, [arXiv:hep-ph/9605323](#).
- [54] S. Catani, S. Dittmaier, M. H. Seymour, and Z. Trocsanyi, Nucl.Phys. **B627** (2002) 189, [arXiv:hep-ph/0201036 \[hep-ph\]](#).
- [55] A. Denner, S. Dittmaier, T. Kasprzik, and A. Mück, JHEP **06** (2011) 069, [arXiv:1103.0914 \[hep-ph\]](#).

- [56] A. Denner, S. Dittmaier, T. Kasprzik, and A. Mück, Eur. Phys. J. **C73** (2013) 2, 2297, [arXiv:1211.5078 \[hep-ph\]](#).
- [57] Particle Data Group, J. Beringer *et al.*, Phys.Rev. **D86** (2012) 010001.
- [58] A. Denner, S. Dittmaier, M. Roth, and D. Wackeroth, Nucl.Phys. **B587** (2000) 67, [arXiv:hep-ph/0006307 \[hep-ph\]](#).
- [59] J. Butterworth *et al.*, [arXiv:1405.1067 \[hep-ph\]](#).
- [60] A. Denner, S. Dittmaier, M. Roth, and D. Wackeroth, Nucl.Phys. **B560** (1999) 33, [arXiv:hep-ph/9904472 \[hep-ph\]](#).
- [61] A. Denner, S. Dittmaier, M. Roth, and L. Wieders, Nucl.Phys. **B724** (2005) 247, [arXiv:hep-ph/0505042 \[hep-ph\]](#).
- [62] A. Denner and S. Dittmaier, Nucl.Phys.Proc.Suppl. **160** (2006) 22, [arXiv:hep-ph/0605312 \[hep-ph\]](#).
- [63] D. Bardin, A. Leike, T. Riemann, and M. Sachwitz, Phys.Lett. **B206** (1988) 539.
- [64] NNPDF Collaboration, R. D. Ball *et al.*, Nucl.Phys. **B877** (2013) 290, [arXiv:1308.0598 \[hep-ph\]](#).
- [65] K.-P. Diener, S. Dittmaier, and W. Hollik, Phys.Rev. **D72** (2005) 093002, [arXiv:hep-ph/0509084 \[hep-ph\]](#).
- [66] S. Dittmaier and M. Huber, JHEP **1001** (2010) 060, [arXiv:0911.2329 \[hep-ph\]](#).
- [67] L. J. Dixon, Z. Kunszt, and A. Signer, Phys.Rev. **D60** (1999) 114037, [arXiv:hep-ph/9907305 \[hep-ph\]](#).
- [68] S. Haywood *et al.*, [arXiv:hep-ph/0003275 \[hep-ph\]](#).
- [69] T. Kinoshita, J.Math.Phys. **3** (1962) 650.
- [70] T. Lee and M. Nauenberg, Phys.Rev. **133** (1964) B1549.
- [71] J. H. Kühn, F. Metzler, A. A. Penin, and S. Uccirati, JHEP **06** (2011) 143, [arXiv:1101.2563 \[hep-ph\]](#).
- [72] K. Hagiwara, R. D. Peccei, D. Zeppenfeld, and K. Hikasa, Nucl.Phys. **B282** (1987) 253.
- [73] G. Gounaris *et al.* 1996. [arXiv:hep-ph/9601233 \[hep-ph\]](#).
- [74] G. J. Gounaris, J. Layssac, and F. M. Renard, Phys. Rev. **D61** (2000) 073013, [arXiv:hep-ph/9910395 \[hep-ph\]](#).
- [75] A. Denner, Fortsch.Phys. **41** (1993) 307, [arXiv:0709.1075 \[hep-ph\]](#).